Nano-Engineered Thermoelectric Materials for Waste Heat Recovery

Mohsin Saleemi

Doctoral Thesis in Materials Chemistry
KTH Royal Institute of Technology
Stockholm, Sweden 2014

TRITA-ICT/MAP AVH Report 2014:12
ISSN 1653-7610
ISRN KTH/ICT-MAP/AVH-2014:12-SE
ISBN 978-91-7595-210-9

KTH School of Information and
Communication Technology
SE-16440, Kista, Sweden.

A dissertation submitted to KTH Royal Institute of Technology, Stockholm, Sweden, in partial fulfillment of the requirements for the degree of Teknologie Doktor (Doctor of Philosophy). The Public defense will take place on 3rd October 2014 at 14:00 p.m. at Sal B, KTH-Electrum, Isafjordagatan 22, Kista.

Cover image: Strategies to improve *ZT* in Bulk Nanostructured TEs

© Mohsin Saleemi, October 2014

Universitetsservice US-AB, Stockholm 2014

"In the name of Allah, most Gracious, most Compassionate".

I dedicate this thesis to my parents and beloved family.

Abstract

Energy crisis and thermal management related issues have been highlighted in the modern century due to escalating demands for energy consumption and global warming from fossil fuels. Sustainable and alternative energy sources are an ever growing global concern. Thermoelectric (TE) materials have gained significant interest, due to effective solid-state energy conversion from waste heat to useful electrical energy and vice versa. Clean, noise-free, and environment-friendly operation of TE devices has triggered great attention in viable technologies including automotive, military equipment, aerospace, and industries to scavenge waste heat into power. To date, conventional TE materials have shown limited energy conversion efficiency, *i.e.* TE Figure of Merit (*ZT*). However, the concept of nanostructuring and development of novel TE materials have opened excellent avenues to improve significantly the *ZT* values. Nano-engineered bulk TE materials allow effective phonon scattering at the high density of grain boundaries, which offer a way of lowering the thermal conductivity.

Large-scale synthesis of TE nanomaterials is a challenge for the TE industry because of expensive fabrication processes involved. This thesis reports several nano-engineering approaches for fabricating large quantities of bulk nanostructured TE materials. We have developed bottom-up chemical synthesis routes, as well as top-down mechanical alloying methodologies, to produce highly pure, homogenous and highly crystalline TE nanomaterials. State of the art chalcogenide, iron antimonide, and silicide based TE materials have been investigated in this thesis. Chalcogenide are the best candidates for TE devices operating at temperature range up to 450 K. Iron antimonide ($FeSb_2$) have shown attractive performance below room temperature. Earth abundant and environment friendly, silicide based materials have better *ZT* performance in the range of 600-900 K. Spark plasma sintering (SPS) was utilized to preserve the nanostructuring and to achieve the highest compaction density. Comprehensive physiochemical characterizations were performed on as-prepared and SPS compacted samples. Detailed TE evaluation of the fabricated materials showed significant improvement in *ZT* for all categories of TE materials.

Keywords: Thermoelectric, Nano-engineering, Bulk nanostructured, Spark plasma sintering, Chalcogenides, Iron Antimonide, Silicides.

List of Papers Included in the Thesis

1. **Mohsin Saleemi**, Muhammet S. Toprak, Shanghua Li, Mats Johnsson, Mamoun Muhammed, *"Synthesis, processing, and thermoelectric properties of bulk nanostructured bismuth telluride (Bi_2Te_3)",* Journal of Materials Chemistry, 22, 2, 725-730, 2012.

2. **Mohsin Saleemi**, Aleksey Ruditskiy, Muhammet S. Toprak, Marian Stingaciu, Mats Johnsson, Ilona Kretzschmar, Alexandre Jacquot, Martin Jägle, Mamoun Muhammed*, "Evaluation of the Structure and Transport Properties of Nanostructured Antimony Telluride (Sb_2Te_3)",* Journal of Electronic Materials, 43, 6, 1927-1932, 2014.

3. **Mohsin Saleemi,** Mohsen Y. Tafti, Alexandre Jacquot, Martin Jägle, Mamoun Muhammed, Muhammet S. Toprak, *"Chemical synthesis of iron antimonide ($FeSb_2$)and its thermoelectric properties",* Manuscript.

4. **Moshin Saleemi**, Muhammet S. Toprak, Stefania Fiameni, Stefano Boldrini, Simone Battiston, Alessia Famengo, Marian Stingaciu, Mats Johnsson, Mamoun Muhammed, *"Spark plasma sintering and thermoelectric evaluation of nanocrystalline magnesium silicide (Mg_2Si)",* Journal of Materials Science, 48, 5, 1940-1946, 2013.

5. Simone Battiston, Stefania Fiameni, **Mohsin Saleemi**, Stefano Boldrini, Alessia Famengo, Filippo Agresti, Marian Stingaciu, Muhammet S. Toprak, Monica Fabrizio, Simona Barison, *"Synthesis and Characterization of Al-Doped Mg_2Si Thermoelectric Materials",* Journal of Electronic Materials, 42, 7, 1956-1959, 2013.

6. Stefania Fiameni, Alessia Famengo, Filippo Agresti, Stefano Boldrini, Simone Battiston, **Mohsin Saleemi**, Mats Jhonsson, Simona Barison, Monica Fabrizio, *"Effect of Synthesis and Sintering Conditions on the Thermoelectric Properties of n-Doped Mg_2Si",* Journal of Electronic Materials, 43, 6, 2301-2306, 2014.

7. Stefania Fiameni, Alessia Famengo, Stefano Boldrini, Simone Battiston, **Mohsin Saleemi**, Marian Stingaciu, Mats Jhonsson, Simona Barison, Monica Fabrizio, *"Introduction of Metal Oxides into Mg_2Si Thermoelectric Materials by Spark Plasma Sintering",* Journal of Electronic Materials, 42, 7, 2062-2066, 2013.

8. Alessia Famengo, Simone Battiston, **Mohsin Saleemi**, Stefano Boldrini, Stefania Fiameni, Filippo Agresti, Muhammet S. Toprak, Simona Barison, Monica Fabrizio, *"Phase Content Influence on Thermoelectric Properties of Manganese Silicide-Based Materials for Middle-High Temperatures",* Journal of Electronic Materials, 42, 7, 2020-2024, 2013.

9. **Mohsin Saleemi**, Muhammet S. Toprak, Stefania Fiameni, Stefano Boldrini, Simone Battiston, Alessia Famengo, Marian Stingaciu, Mats Johnsson, Mamoun Muhammed, *"Thermoelectric performance of higher manganese silicides nanocomposites"*, Accepted in Journal of Alloys and Compounds

Author's Contribution

Paper 1: Complete planning of the experiments, performing all the experiments, performing all physico-chemical characterization, analyzing materials characterization data, writing the complete manuscript.

Paper 2: Complete planning of the experiments, performing most of the experiments, performing physico-chemical characterization, analyzing materials characterization data, writing the complete manuscript.

Paper 3: Complete planning of the experiments, performing all the experiments, performing all physico-chemical characterization, analyzing materials characterization data, writing the complete manuscript.

Paper 4: Complete planning of the experiments, performing part of the experiments, performing all physico-chemical characterization, analyzing materials characterization data, writing the complete manuscript.

Paper 5: Planning major part of the experiments, performing major part of the experiments related to SPS compaction and material characterization, writing part of the manuscript.

Paper 6: Planning some part of the experiments, performing part of the experiments related to SPS compaction and material characterization, writing part of the manuscript.

Paper 7: Planning major part of the experiments, performing part of the experiments, performing part of physico-chemical characterization, analyzing materials characterization data, writing the complete manuscript.

Paper 8: Planning major part of the experiments, performing part of the experiments, performing part of physico-chemical characterization, analyzing materials characterization data, writing the complete manuscript.

Paper 9: Complete planning of the experiments, performing all the experiments, performing all physico-chemical characterization, analyzing materials characterization data, writing the complete manuscript.

Other Work not included in the Thesis

1. Abdullah Khan, **Mohsin Saleemi**, Mats Johnsson, Li Han, Nong V. Nong, Mamoun Muhammed , Muhammet S. Toprak, *"Fabrication, spark plasma consolidation, and thermoelectric evaluation of nanostructured $CoSb_3$",* Journal of Alloys and Compounds, 612, 5, 293-300, 2014.
2. Mohsen Y. Tafti, **Mohsin Saleemi**, Muhammet S. Toprak, Mats Johnsson, Alexandre Jacquot, Martin Jägle, Mamoun Muhammed, *"Fabrication and characterization of nanostructured thermoelectric $Fe_xCo_{1-x}Sb_3$",* in press in Central European Journal of Chemistry.
3. **Mohsin Saleemi**, Mohsen Y. Tafti, Muhammet S. Toprak, Marian Stingaciu, Mats Johnsson, Martin Jägle, Alexandre Jacquot, Mamoun Muhammed, *"Fabrication of nanostructured bulk cobalt antimonide ($CoSb_3$) based skutterudites via bottom-up synthesis",* MRS Proceedings 1490, 121-126, 2013.
4. Alexandre Jacquot, Marta Rull, Alberto Moure, J. F. Fernandez-Lozano, Marisol Martin-Gonzalez, **Mohsin Saleemi**, Muhammet S. Toprak, Mamoun Muhammed, Martin Jägle, *"Anisotropy and inhomogeneity measurement of the transport properties of spark plasma sintered thermoelectric materials",* MRS Proceedings 1490, 89-95, 2013.
5. Mohsen Y. Tafti, **Mohsin Saleemi**, Alexandre Jacquot, Martin Jägle, Mamoun Muhammed, Muhammet S. Toprak, *"Fabrication and characterization of nanostructured bulk skutterudites",* MRS Proceedings 1543, 105-110, 2013.
6. **Mohsin Saleemi**, Muhammet S. Toprak, Shanghua Li, Mats Johnsson, Mamoun Muhammed, *"Fabrication and Spark plasma sintering of nanostructured bismuth telluride (Bi_2Te_3)",* AIP Conference Proceedings 1449, 115-118, 2012.
7. **Mohsin Saleemi**, Srinivas Vanapalli, Nader Nikkam, Muhammet S. Toprak, Mamoun Muhammed, *"Classical behavior of alumina (Al_2O_3) nanofluids in Antifrogen N with experimental evidence",* Manuscript.
8. Nader Nikkam, **Mohsin Saleemi**, Muhammet S. Toprak, S. Li, Mamoun Muhammed, Ehsan B. Haghighi, Rahmatollah Khodabandeh, and Björn Palm, *"Novel Nanofluids Based on Mesoporous Silica for Enhanced Heat Transfer",* Journal of Nanoparticle Research, 13, 6201-6206, 2011.
9. Ehsan B. Haghighi, **Mohsin Saleemi**, Nader Nikkam, Rahmatollah Khodabandeh, Muhammet S. Toprak, Mamoun Muhammed, Björn Palm, *"Accurate basis of comparison for convective heat transfer in nanofluids",* International Communications in Heat and Mass Transfer, 52, 1-7, 2014.
10. Ehsan B. Haghighi, **Mohsin Saleemi**, Nader Nikkam, Rahmatollah Khodabandeh, Muhammet S. Toprak, Mamoun Muhammed and Björn Palm, *"Cooling performance of nanofluids in a small diameter tube",* Experimental Thermal and Fluid Science, 49, 114–122, 2013.
11. Mariam Jarahnejad, Ehsan B. Haghighi, **Mohsin Saleemi**, Nader Nikkam, Rahmatollah Khodabandeh, Björn Palm, Muhammet S. Toprak and Mamoun

Muhammed, *"The Experimental investigation of effective parameters on viscosity of water based Al_2O_3 and TiO_2 nanofluids",* Submitted.

12. Ehsan B. Haghighi, Nader Nikkam, **Mohsin Saleemi**, Mohammad Reza Behi, Seyed A. Mirmohammadi, Heiko Poth, Rahmatollah Khodabandeh, Muhammet S. Toprak, M. Muhammed and Björn Palm, *"Shelf Stability of Nanofluids and Its Effect on Thermal Conductivity and Viscosity",* Measurement Science and Technology, 24, 105301- 105301-11, 2013.
13. Nader Nikkam, Morteza Ghanbarpor, **Mohsin Saleemi**, Muhammet S. Toprak, Mamoun Muhammed and Rahmatollah Khodabandeh, *"Thermal and rheological properties of micro- and Nanofluids of copper in diethylene glycol – as heat exchange liquid",* MRS Proceedings of the Symposium on Nanoscale Heat Transport—From Fundamentals to Devices, 1543, 165-170, 2013.
14. Nader Nikkam, Morteza Ghanbarpour, **Mohsin Saleemi**, Ehsan B. Haghighi, Rahmatollah Khodabandeh, Mamoun Muhammed, Björn Palm and Muhammet S. Toprak, *"Experimental investigation on thermo-physical properties of copper/diethylene glycol nanofluids fabricated via microwave-assisted route",* Applied Thermal Engineering, 65, 158-165, 2014.
15. Nader Nikkam, **Mohsin Saleemi**, Ehsan B. Haghighi, Morteza Ghanbarpour, Rahmatollah Khodabandeh M. Muhammed, Björn Palm and Muhammet S. Toprak, *"Fabrication, characterization and thermo-physical property evaluation of water/ethylene glycol based SiC nanofluids for heat transfer applications",* Nano-Micro Letters, 6, 178-189, 2014.
16. Nader Nikkam, Ehsan B. Haghighi, **Mohsin Saleemi**, Mohammadreza Behi, Rahmatollah Khodabandeh, Mamoun Muhammed, Björn Palm and Muhammet S. Toprak, *"Experimental Study on Preparation and Base Liquid Effect on Thermo-physical Characteristics of α-SiC Nanofluids",* International Communications in Heat and Mass Transfer, 52, 1–7, 2014.
17. Terrance Burks, Abdusala*m Uheida,* **Mohsin Saleemi**, Muhammed Eita, Muhammet S. Toprak, Mamoun Muhammed, *"Removal of Chromium(VI) Using Surface Modified Superparamagnetic Iron Oxide Nanoparticles*", Separation Science and Technology, 48, 8, 1243-1251, 2013.

Patents

1. Nader Nikkam, **Mohsin Saleemi**, Muhammet S. Toprak, Shanghua Li and Mamoun Muhammed, (Granted) "*The Use of a Suspension Comprising Mesoporous Silica Particles As Heat Exchange Fluids",* (Swedish Patent number: SE1000924-9), IPC (International Patent Classification): C01B33/141, C08K3/36, C09K5 /00.
2. **Mohsin Saleemi**, Nader Nikkam, Mohammad Reza Behi, Ehsan B. Haghighi, Muhammet S. Toprak, Rahmatollah Khodabandeh and Mamoun Muhammed, (Pending) *"Method and Apparatus for Simple Determination of The Stability of Suspensions",* (Swedish patent application number: 1100961-0).

Conference Presentations

1. Muhammet S. Toprak, **Mohsin Saleemi**, Shanghua Li, Mats Johnsson and Mamoun Muhammed, *"Bulk nanostructured Thermoelectric materials",* 10th International Conference on Nanostructured Materials, Sep 13-17, 2010, Rome, Italy. (Oral)
2. Nader Nikkam, **Mohsin Saleemi**, Muhammet S. Toprak, Shanghua Li, Ehsan B. Haghighi, Rahmatollah Khodabandeh, Mamoun Muhammed and Björn Palm, *"Novel Nanofluids Based on Mesoporous Silica for Enhanced Heat Transfer",* 10th International Conference on Nanostructured Materials, Sep 13-17, 2010, Rome, Italy. (Poster)
3. **Mohsin Saleemi**, Nader Nikkam, Muhammet S. Toprak, Shanghua Li, Ehsan B. Haghighi, Rahmatollah Khodabandeh, Mamoun Muhammed and Björn Palm, *"Ceria Nanofluids for Efficient Heat Management",* 10th International Conference on Nanostructured Materials, Sep 13-17, 2010, Rome, Italy. (Poster)
4. Muhammet S. Toprak, **Mohsin Saleemi** and Mamoun Muhammed, *"Bulk Nanostructured Thermoelectric Bismuth Telluride",* 7th Nanoscience and Nanotechnology Conference, 27 Jun- 1 Jul, 2011, Istanbul, Turkey. (Oral)
5. **Mohsin Saleemi**, Nader Nikkam, Muhammet S. Toprak, Ehsan B. Haghighi, Rahmatollah Khodabandeh, Mamoun Muhammed and Björn Palm, *"One Step synthesis of Ceria (CeO_2) Nanofluids with enhanced thermal transport Properties",* 7th Nanoscience and Nanotechnology Conference, 27 Jun- 1 Jul, 2011, Istanbul, Turkey. (Poster)
6. Nader Nikkam, **Mohsin Saleemi**, Muhammet S. Toprak, Ehsan B. Haghighi, Rahmatollah Khodabandeh, Mamoun Muhammed and Björn Palm, *"Microwave-assisted Synthesis of Copper Nanofluids for Heat Transfer Applications",* 7th Nanoscience and Nanotechnology Conference, 27 Jun- 1 Jul, 2011, Istanbul, Turkey. (Poster)
7. Nader Nikkam, **Mohsin Saleemi**, Muhammet S. Toprak, Ehsan B. Haghighi, Rahmatollah Khodabandeh, Mamoun Muhammed and Björn Palm, *"Rheological Properties of Copper Nanofluids Synthesized by Using Microwave-Assisted Method",* 4th International conference on nanostructures, ICNS4, 12-14 March, 2012, Kish Island, Iran. (Oral)
8. **Mohsin Saleemi**, Muhammet S. Toprak, Stefania Fiameni, Stefano Boldrini, Simone Battiston, Alessia Famengo, Marian Stingaciu, Mats Johnsson and Mamoun Muhammed, *"Spark Plasma Sintering and Thermoelectric Evaluation of Nanostructured Magnesium Silicide (Mg_2Si)",* European Materials Research Society Conference (EMRS), May 14-18, 2012, Strasbourg, France. (Oral)
9. Nader Nikkam, **Mohsin Saleemi**, Muhammet S. Toprak, Ehsan B. Haghighi, Rahmatollah Khodabandeh, Mamoun Muhammed and Björn Palm, *"Effect of nanoparticle morphology on thermal conductivity and rheology of Zinc Oxide nanofluids",* European Materials Research Society Conference (EMRS), May 14-18, 2012, Strasbourg, France. (Poster)

10. Nader Nikkam, Sathya P. Singh, **Mohsin Saleemi**, Muhammet S. Toprak, Rahmatollah Khodabandeh, Mamoun Muhammed and Björn Palm, *"A comparative study of rheological properties and thermal conductivity of silver nanofluids in water and ethylene glycol base fluids",* 8th Nanoscience and Nanotechnology Conference, June 25-29, 2012, Ankara, Turkey. (Poster)
11. **Mohsin Saleemi**, Marian Stingaciu, Mohsen Y. Tafti, Muhammet S. Toprak, Mats Johnsson, Marisol S. Martín-Gonzalez, P. Diaz-Chao, Martin Jägle, Alexandre Jacquot and Mamoun Muhammed. *"Novel Synthesis Approach for Cobalt Antimonide ($CoSb_3$) Thermoelectric Material by Sol-Gel Precursor Route",* International and European Conference on Thermoelectrics 2012, Jul 9-12, 2012, Aalborg, Denmark. (Poster)
12. Mohsen Y. Tafti, **Mohsin Saleemi**, Muhammet S. Toprak, Mamoun Muhammed Marian Stingaciu, Mats Johnsson, Martin Jägle, Alexandre Jacquot Marisol S. Martín-Gonzalez and P. Diaz-Chao, *"A comparative study of $Co_{1-x}Fe_xSb_3$ synthesized via solid state and chemical co-precipitation precursor routes",* International and European Conference on Thermoelectrics 2012, Jul 9-12, 2012, Alborg, Denmark. (Oral)
13. Ehsan Bitaraf Haghighi, M. Ghadamgahi, Mohammadreza Behi, Seyed A. Mirmohammadi, Rahmatollah Khodabandeh, Björn Palm, **Mohsin Saleemi**, Nader Nikkam, Muhammet S. Toprak and Mamoun Muhammed, *"Measurement of temperature-dependent viscosity of nanofluids and its effect on pumping power in cooling systems",* 6th European Thermal Sciences Conference (Eurotherm 2012), September 4-7, 2012, Poitiers, France. (Poster)
14. Alexandre Jacquot,Marisol S. Martín-Gonzalez, **Mohsin Saleemi**, Muhammet S. Toprak, Mamoun Muhammed and Martin Jägle, *"Anisotropy and Inhomogeneity Measurement of the Transport Properties of Spark Plasma Sintered Thermoelectric",* Materials Research Society (MRS) Conference Fall 2012, Nov 25-30, 2012, Boston, USA. (Oral)
15. **Mohsin Saleemi**, Mohsen Y. Tafti, Marian Stingaciu, Mats Johnsson, Martin Jägle, Alexandre Jacquot, M. Muhammed, *"Fabrication of Nanostructured Bulk Cobalt Antimonide ($CoSb_3$) Based Skutterudites via Bottom-up Synthesis",* Materials Research Society (MRS) Conference Fall 2012, Nov 25-30, 2012, Boston, USA. (Poster; Award for Best Poster)
16. **Mohsin Saleemi**, Mohsen Y. Tafti, Muhammet S. Toprak, Martin Jägle, Alexandre Jacquot, Mats Johnsson and Mamoun Muhammed, *"Fabrication and Characterization of Nanostructured Bulk Skutterudites",* Materials Research Society Conference, MRS, April 1-5, 2013, San Francisco, USA. (Poster)
17. Nader Nikkam, **Mohsin Saleemi**, Ehsan B. Haghighi, Morteza Ghanbarpour, Muhammet S. Toprak, Rahmatollah Khodabandeh, Mamoun Muhammed and Björn Palm, *"Nano-engineered SiC Heat Transfer Fluids for Effective Cooling",* Materials Research Society Conference, Materials Research Society Conference, MRS, April 1-5, 2013, San Francisco, USA. (Oral)

18. **Mohsin Saleemi**, Mohsen Y. Tafti, Muhammet S. Toprak, Martin Jägle, Alexandre Jacquot, Mats Johnsson and Mamoun Muhammed, *"Chemical synthesis and thermoelectric evaluation of nanostructured iron antimonide ($FeSb_x$)",* European Materials Research Conference, EMRS, May 27-31, 2013, Strasbourg, France. (Poster; Award for Best Paper)
19. Nader Nikkam, **Mohsin Saleemi**, Ehsan B. Haghighi, Morteza Ghanbarpour, Muhammet S. Toprak, Rahmatollah Khodabandeh, Mamoun Muhammed and Björn Palm, *"Design and Fabrication of Efficient Nanofluids Based on SiC Nanoparticles for Heat Exchange Applications",* European Materials Research Conference, EMRS, May 27-31, 2013, Strasbourg, France. (Poster)
20. **Mohsin Saleemi**, Nader Nikkam, Milad G. Yazdi, Muhammet S. Toprak and M. Muhammed, *"Effect of particles size and surface modification on thermal conductivity and viscosity of alumina nanofluids",* European Materials Research Conference, EMRS, May 27-31, 2013, Strasbourg, France. (Poster)
21. **Mohsin Saleemi**, Muhammet S. Toprak, Simone Battiston, Mats Johnsson, Stefania Fiameni, Stefano Boldrini and Alessia Famengo, *"Ytterbium (Yb) doped nanostructured higher manganese silicide (HMS) for thermoelectric applications",* International Conference on Thermoelectrics ICT 2013, June 30 - July 4, 2013, Kobe, Japan. (Oral)
22. **Mohsin Saleemi**, A Ruditskiy, Muhammet S. Toprak, Marian Stingaciu, Mats Johnsson, Ilona Kretzschmar, Alexandre Jacquot, Martin Jägle and Mamoun Muhammed, *"Structural and Transport Property Evaluation of Nanosized Antimony Telluride (Sb_2Te_3) Fabricated by Solution Precursor Route",* International Conference on Thermoelectrics ICT 2013, June 30 - July 4, 2013, Kobe, Japan. (Poster)
23. Simone Battiston, Stefania Fiamen, Stefano Boldrini, Alessia Famengo, **Mohsin Saleemi**, Mats Johnsson, Muhammet Toprak, Monica Fabrizio and Simona Barison *"Influence of the Al and Mg content on the thermoelectric properties of higher manganese silicides obtained by one step synthesis and sintering",* International Conference on Thermoelectrics ICT 2013, June 30 - July 4, 2013, Kobe, Japan. (Poster)
24. Ehsan B. Haghighi, Morteza Ghanbarpour, **Mohsin Saleemi**, Nader Nikkam, Rahmatollah Khodabandeh, Muhammet S. Toprak, Mamoun Muhammed and Björn Palm, *"Measurement of temperature-dependent viscosity of nanofluids and its effect on pumping power in cooling systems",* International Conference on Applied energy, ICAE2013, July 1-4, 2013, Pretoria, South Africa. (Oral)
25. **Mohsin Saleemi**, Simone Battiston, Alessia Famengo, Stefania Fiameni, Stefano Boldrini, Mats Johnsson, and Mamoun Muhammed and Muhammet S. Toprak, *"Nanostructured silicide based materials for thermoelectrics applications",* International Scientific Spring 2014, March 10-14, 2014, Islamabad, Pakistan. (Oral; Award for Best Talk)

26. **Mohsin Saleemi** and Muhammet S. Toprak, *"Nano-Engineered Materials for Sustainable Energy applications",* Nano-SET 2014, March 17-20, 2014, Lahore, Pakistan. (Invited Talk)

List of Abbreviations and Symbols

BM	Ball Milling
DSC	Differential Scanning Calorimetry
EDX	Energy Dispersive X-ray Spectroscopy
EBSD	Electron Backscatter Diffraction
FESEM	Field Emission Scanning Electron Microscopy
MA	Mechanical Alloying
NC	Nanocomposites
NM	Nanomaterial
NS	Nanostructured
PGEC	Phonon Glass - Electron
S	Seebeck Coefficient
SEM	Scanning Electron Microscope
SPS	Spark Plasma Sintering
TE	Thermoelectric
TEs	Thermoelectrics
TEM	Transmission Electron Microscope
TGA	Thermal Gravimetric Analysis
XRD	X-ray Diffraction
ZT	Thermoelectric Figure of Merit
S	Seebeck Coefficient
ρ	Electrical Resistivity
σ	Electrical Conductivity
κ	Thermal Conductivity
κ_{el}	Electronic Thermal Conductivity
κ_{latt}	Lattice Thermal Conductivity
$S^2\sigma$	Power Factor
I	Current
$\prod$	Peltier Coefficient
ΔV	Voltage Difference
ΔT	Temperature Difference

Table of Contents

Abstract i
List of Papers Included in the Thesis ii
Author's Contribution iv
Other Work not included in the Thesis v
Patents vi
Conference Presentations vii
List of Abbreviations and Symbols xi
1 Introduction 1
1.1 Nanotechnology and Nanomaterials 2
1.2 Thermoelectric (TE) Materials 3
1.2.1 Applications of TE Devices 3
1.2.2 Thermoelectric Effects 4
1.2.3 n-type and p-type TE Materials 5
1.2.4 Challenges in Thermoelectric Research 6
1.2.5 A Brief History of TE Materials 7
1.2.6 Figure of Merit in TE materials 9
1.3 Strategies for Improving ZT 10
1.3.1 Nanostructured Bulk Thermoelectrics (TEs) 10
1.3.2 Nano-engineered Bulk TEs 11
1.3.3 Nano-composite Bulk TEs 12
1.4 TE Materials Synthesis 12
1.4.1 Top-Down Approach 13
1.4.2 Bottom-Up Approach 13
1.5 Representative high-performance TE materials 13
1.5.1 Chalcogenides based Alloys 14
1.5.2 Silicide based Alloys 14
1.5.3 Iron Antimonide ($FeSb_2$) 15
1.6 Objectives 15
2 Experimental Methods 17
2.1 Materials Synthesis 17
2.1.1 Chemical Synthesis of Chalcogenides 17
2.1.2 Mechanical Alloying of Silicides 19

2.2 Spark Plasma Sintering (SPS) 21
2.2.1 Optimizations of SPS Parameters 21
2.3 Characterizations 22
2.3.1 Crystal Structure Characterization 22
2.3.2 Microstructure Characterization 22
2.3.3 Thermal Characterization 23
2.3.4 TE Transport Characterization 23
3 Results and Discussions 24
3.1 Chalcogenide Based Materials 24
3.1.1 n-type Chalcogenides (Paper I) 24
3.1.2 p-type Chalcogenides (Paper II) 27
3.2 $FeSb_2$ based Material (Paper III) 29
3.3 Silicides based Materials 30
3.3.1 n-type Silicides (Paper IV) 31
3.3.2 p-type Silicides (Paper VIII) 35
4 Conclusions 39
5 Future Work 42
Acknowledgements 44
References 46

Chapter 1

1 Introduction

For the first time in the earth's history, we are facing global energy crisis due to the huge consumption of non-renewable resources (fossil fuels). In august 2014, the *Global Footprint Network* have published a report, stated that earth population have consumed its annual resources stock, such as water, food and energy,[1] which means for the rest of the year 2014, the world will maintain ecological deficit for the natural resources. Also some reports critically point out, oil and gas reserves may diminish in the coming 50 years.[2] In recent years, burning of fossil fuels has also affected our climate. Carbon dioxide emissions have reached a record level in the last decade, which is an alarming fact. Scientific evidence has supported the argument that there is an urgent need to establish concerted policies to prevent our environment from catastrophic situations.[3] One possible solution to reduce the emergent energy demand is through increased efficiency and conservation of produced energy. Secondly, to meet future energy challenges, the need to develop and research a broad range of renewable and sustainable energy sources to decrease the climate change threats is paramount. Evolutionary renewable technologies such as solar, wind, biomass, and bio fuels need to be further developed. Moreover, sustainability and energy conservation is an issue that can be addressed for all the emerging technologies.[4–6]

1.1 Nanotechnology and Nanomaterials

Nanotechnology is a branch of science and engineering which utilizes the nanometer scale (10^{-9} meters) in manufacturing of structures and devices. Researchers and scientists have been developing the ability to manipulate the single atom and/or small group of atoms for startling applications with significantly influenced characteristics including mechanical, optical, electrical, and thermal properties.[7] Nanosciences have successfully demonstrated that the unique properties of the material can be obtained in order to develop new capabilities and potential applications. In particular, materials for renewable energy have attracted great attention in this area due to improved efficiency in the working devices.[7] Whereas, solar power conversion efficiency has been increased from 4 to 14 % by using nano-engineered surfaces. However, new synthesis routes coupled with the aid of nanotechnology may develop a novel understanding about the enhanced characteristics of present materials [8], which results in a technical revolution, which will impact both short and long term endeavors. Figure 1.1 describes different nanomaterials architectures, classified based on the number of degrees of freedom of charge carriers, depending upon their dimensionalities.[9] By way of illustration, charge carriers in a nanoparticle or quantum structure are confined in three dimensions which corresponds to 0D; nanowires and thin film structures are confined in 2 and 1 dimensions respectively, referred to as 1D and 2D.[10] However, the large size crystals, bulk nanostructures, with nano building blocks are the ones, which are known as 3D-bulk structures.[11] Among these classified nanomaterials, bulk nanomaterials (NM) are possible to be fabricated in large scale rather than nanofabrication methods commonly used by semiconductor industry.[12,13]

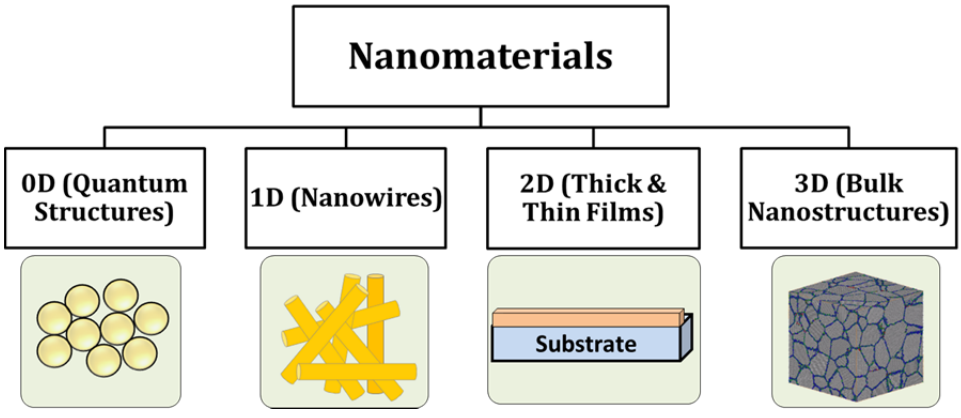

Figure 1.1 *Nanomaterials classification*

1.2 Thermoelectric (TE) Materials

Recently, TE materials have attracted extensive interest as an alternative energy source because of their capability of direct conversion between heat and electricity.[11] TE generators (TEGs) have the ability to harvest useful electrical energy from waste heat. TEGs possess several advantages such as: solid state direct inter conversion, compact structure, noise-free, operational without any moving parts and/or any hazardous working fluids.[14–17] However, TEGs are available in a rather limited market due to the high cost of available TE materials and their low efficiency. Therefore, research on improving the efficiency of TE materials and reducing their cost is highly demanded.[18] Performance of TE materials can be enhanced via nanotechnology approaches through novel compositions, low dimensionality, and innovative device design.[19–21]

1.2.1 Applications of TE Devices

TE devices have attracted increasing attention as sustainable and alternate energy resources. Furthermore, miniaturization of sensors and electronic circuits have increased the challenges for heat management using TE systems, as excessive heat often causes failure of the device, is one example of the important application areas of TE devices.[22,23] TE devices can provide the best solutions for heat management of such systems.[24] Second major application for TE systems can be seen in power generation as TEGs, which utilize waste heat to directly produce useful electric power.[25] It is reported that more than 60 % of primary energy is wasted as heat in the combustion process. This considerable amount of energy loss causes a high impact on our environment. The automotive industry can benefit by utilizing the waste heat from the exhaust pipe and converting it to the power for charging car's battery or running electrical utilities in the car.[26,27] This process will improve the fuel-efficiency and reduce environmental impact of automobiles. TEGs can also utilize the

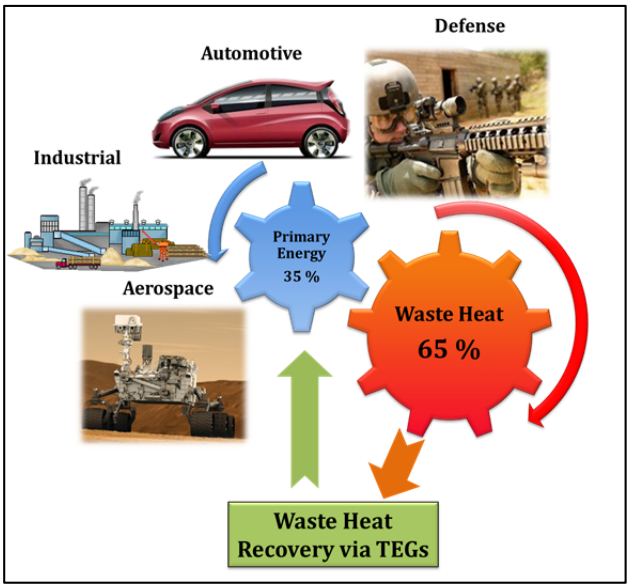

Figure1.2 *Industrial Waste Heat Recovery*

waste heat from human body to power some electronic gadgets such as a quartz wrist watch that requires only 20-40 μW. Seiko and Citizen have installed TEGs to harvest ambient heat for powering their watches.[28] TEGs can also be used in human body implants to power medical devices. Currently, many industries use furnaces and chimneys that require very high temperature and release waste heat that can be captured to recover for production of electricity.[29] Similarly, it is very useful for frontier areas such as applications within the aerospace industry where the conservation and conversion of energy is an insurmountable engineering challenge. Figure 1.2 displays some examples for waste heat recovery in different industries.

1.2.2 Thermoelectric Effects

Temperature gradient across a TE material can generate electricity; charge carriers (electrons and holes) diffuse across a hot source to a cold source can be attributed to their high energy in the hot regime.[19] Thus, a charge difference built up between the hot and cold side produces voltage and electric current. Fundamental physical phenomena are required to understand the TE effect.[11]

1.2.2.1 Seebeck Effect

In 1821, Thomas Johann Seebeck discovered a potential difference (ΔV) was generated when two dissimilar materials were joined together while two ends were held at different temperatures. Mathematically, the Seebeck effect can be described as, $S = -\Delta V/\Delta T$, where S is the Seebeck coefficient, ΔV is the voltage difference and ΔT is the temperature difference between hot and cold sides of the junction. Seebeck coefficient is denoted by a negative value for n-type semiconductors, when the electrons diffuse from hot end to the cold end; and by a positive value for p-type semiconductors when the holes diffuse from hot end to the cold end, *i.e.* electrons move in the opposite direction.[19],[24]

1.2.2.2 Peltier Effect

An electrical current can generate or remove heat at the junctions of two dissimilar conducting materials. This theory was developed, in 1834, by French scientist Jean Charles Peltier. When a current ***I***, passes through a circuit made of two different materials A and B, the evolution of heat may occur at junction A and absorbed at junction B. Therefore, Peltier heat absorbed at the junction can be measured with the help of, $Q = \prod.I$, where Q is the heat absorbed which is directly proportional to the

current (I) and Peltier coefficient ($\prod$) of the materials used in the circuit.[11,19] Furthermore, Lentz explained the true nature of the Peltier effect, in 1838, when a current flows through a conducting circuit, heat is either absorbed or generated.

1.2.2.3 Thomson Effect

Seebeck and Peltier effects were combined in a third TE effect known as Thomson effect, presented by Lord Kelvin in 1851. He described the heating or cooling of a homogenous conducting material when an electric current passes through it in the presence of a temperature gradient.[11] As further seen in the example that the Seebeck coefficient is not constant at different temperatures in many conducting materials. Thus, a longitudinal temperature gradient will cause a gradient in the Seebeck coefficient resulting in the Peltier effect while a current is driven through this gradient.[11]

1.2.2.4 TE Figure of Merit

Performance of TE materials is determined by the physical transport properties. It is denoted as the dimensionless TE figure of merit (ZT), which is expressed as follows:

$$ZT = \frac{S^2 \sigma T}{\kappa}$$

where, S is the Seebeck coefficient, σ is the electrical conductivity, κ is the thermal conductivity, and T is the absolute temperature. To obtain improved ZT, higher σ and a large S is required to generate large output power while minimum κ is favorable for maintaining large temperature gradients across the two ends (hot and cold). However, κ consists of electronic (κ_{el}) and lattice (κ_{latt}) components and total κ is the sum of both components ($\kappa = \kappa_{el} + \kappa_{latt}$). Recently, many reports demonstrated that the reduction in lattice thermal conductivity helps to reduce the κ and improves the overall ZT.[11,15,19]

1.2.3 n-type and p-type TE Materials

TE devices consist of different materials, one with dominantly negative free charge carriers (electrons), defined as n-type, and other with dominantly positive charge carriers (holes) referred to as p-type. Figure 1.3 (a-b) illustrates the simplest schematic of a TEG generator and Peltier cooling device containing n- and p-type legs which are connected electrically in series and thermally in parallel. In power generation modules, a voltage difference proportional to the temperature gradient

will result in a current flow that generates electric power; it is the product of voltage and electrical current across the hot and cold sides.[30] TEGs have internal resistance mainly due to resistance of TE materials, which may cause a voltage drop when the load is reduced. However, maximum efficiency can be obtained when the internal resistance and the load are nearly equal because it will give maximum output power attained from the load. While in a refrigeration module, load is applied via external source (*e.g.* battery) to drive heat via charge carriers (electrons and/or holes) from one source to the other.[24,30] Performance of the Peltier device also relies on the efficiency of TE materials as large figure of merit suggests improved efficiency of TE materials.

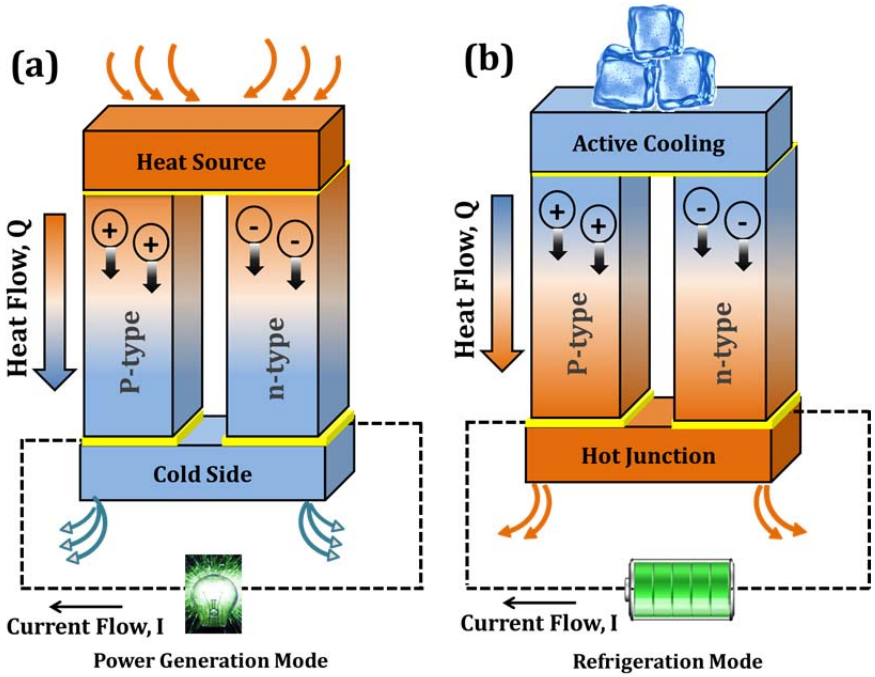

Figure 1.3 *Schematic Illustration of TE devices (a) Power Generating Module, (b) Refrigeration Module (adopted from Li et. al.*[30]*)*

1.2.4 Challenges in Thermoelectric Research

Primary scope of TE research is evident to attain improved *ZT* values. Over several decades, it has marginally increased.[15] This section will discuss in detail the major challenges for TEs and possible routes to obtain desirable efficiency from TE materials, and eventually devices. Unfortunately, there is no single material available in nature that has proven to be a good TE candidate. Major challenge resides in three interconnected physical properties used to calculate *ZT, i.e. S*, σ and κ. In order to obtain a high *ZT* value, *S* and σ should be high while κ should be reduced.[19] Their

interdependence have hindered the development and limited the selection of materials for TE applications, as shown in the Figure 1.4.[16] Metals possess a high σ and a high κ, but the power factor ($S^2\sigma$) is rather small. Hence, the overall ZT remains low. On the other hand, insulators are poor thermal and electrical conductors, while semiconductors and semi-metals exhibit large thermopower, relatively high σ, and lower κ that may lead to an optimum ZT value.[15]

When TE materials are integrated into devices, other challenges are inherited such as the coupling of n- and p-type materials with metallic contacts, ceramic plates on both ends, and coefficient of thermal expansion for materials. These challenges are the major parameters in the design of a TE device.[11] Packaging of TE device is another issue, for example for air sensitive TE materials, the device should be sealed in an inert atmosphere. Also, the planar or tubular design may be preferred depending upon the target application.[11]

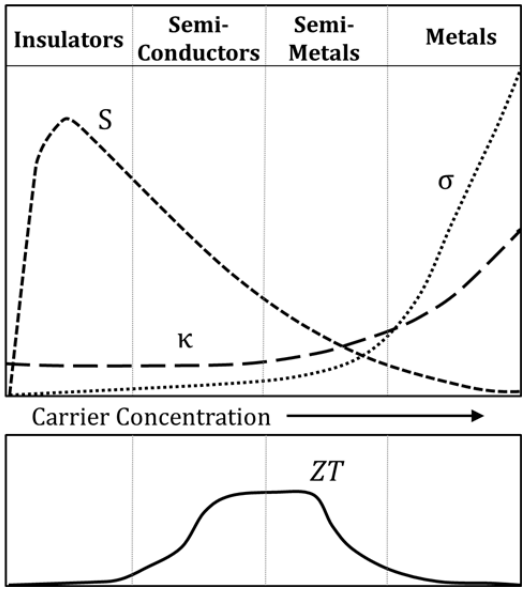

Figure 1.4 *Thermoelectric behavior of different classes of materials*[17]

1.2.5 A Brief History of TE Materials

TE materials have been extensively studied since the 20th century. It is important to revisit the history and development in TEs to understand better how we may be able to tune the ZT. Seebeck, Peltier and Thompson effects were developed on the basis of metals as thermo-elements. However, *Altenkrich* explained theoretical predictions for TE devices which clearly state that metals were inefficient for TE applications.[31,32] *Ioffe* investigated III-V and II-VI semiconductors as TE materials,

he identified n- and p-type semiconductors to form a prototype TE generator.[21] Goldsmid and Wright also contributed to finding the best semiconductor such as Bismuth telluride (Bi_2Te_3) for TE devices.[33,34] They are known as the first generation TEs with an average *ZT* about 1.0 and their device energy conversion efficiency is 4-6%. During the 1950s and beyond, TE research was severely hindered due to the degradation of efficiency of TE materials.

In 1980s, Rowe and his co-workers proposed that phonon scattering at the grain boundaries may improve TE performance.[35] *Dresselhaus and Hicks* revived the nanostructuring concept by explaining the quantum confinement effect causing the enhanced $S^2\sigma$.[36] Their work triggered investigation on low dimensional TE materials, such as superlattices. This approach decreased the lattice thermal conductivity due to the utilization of nanoscale precipitates, grain boundary inclusions, and compositional inhomogeneity.[25,37–39] A wide variety of research activities led to almost doubling the *ZT* at high temperatures. Moreover, it is defined as the second generation of bulk TEs namely clathrates, half-Heuslers, lead tellurides (LAST), and skutterudite compounds have shown *ZT* values up to 1.7 at high temperatures while the conversion efficiency of devices from such materials is about 10-12 %.[25],[40]

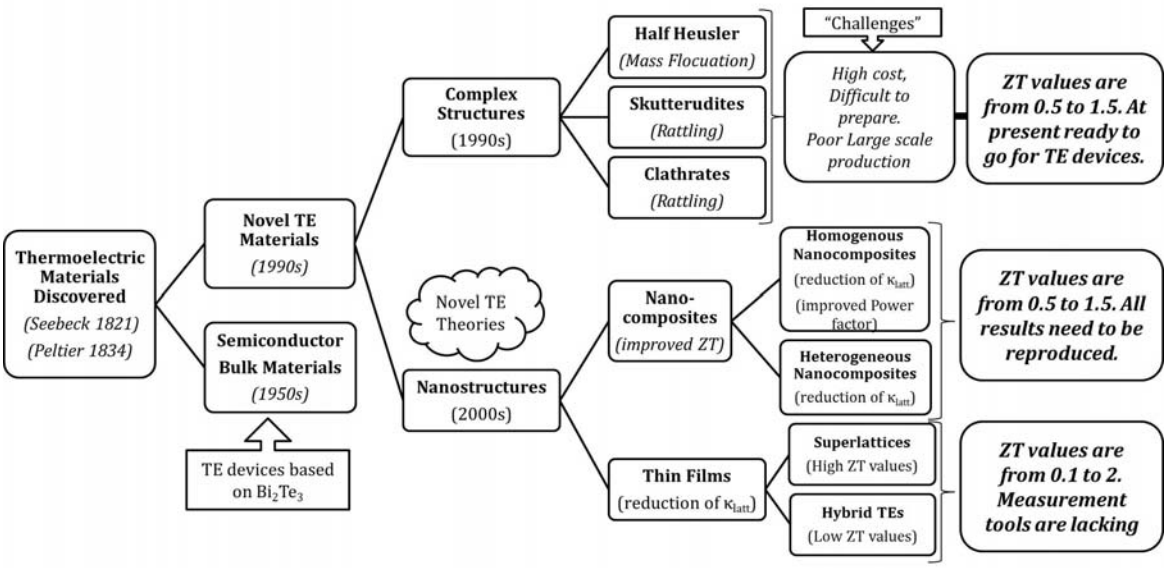

Figure 1.5 *Schematic illustration current state of the art ZT achievements in bulk TEs*

Now thermoelectric researchers are developing third generation TE materials by using many cutting-edge approaches to enhance the *ZT* values in different TE

systems. Researchers are expecting *ZT* values of 1.5 to 2.2 for these materials, which will translate to 15 % conversion efficiency. It is also important to note that some of the recently reported high *ZT* values have not been verified.[14,41–43] Figure 1.5 illustrates the comprehensive landscape of different TE materials established.[11] It describes the revival of TEs with nanostructuring effects that have shown improved TE performance in various material classes. Most of these materials are not available commercially due to small-scale production, high cost, and complications during device fabrication. Large quantities of TE materials and efficient design of TE devices are major challenges at present. Many reports have documented poor mechanical properties of TE materials as well.[11],[18] Due to all of these challenges, to date only bismuth telluride (Bi_2Te_3) based TE modules are available on the market for low grade energy harvesting and cooling purposes.[44]

1.2.6 Figure of Merit in TE materials

Typically, TE materials are categorized on the basis of their application temperature range. In particular, transport properties of TE materials depend on temperature. A limited number of TE materials are appropriate for low temperatures, while other materials are good at intermediate and high temperatures.[45] TE materials suitable at very low temperatures, 4 to 250 K, can be classified as cryogenic temperature range materials. These types of materials are well known for Peltier refrigeration devices. For example, cesium bismuth telluride ($CsBi_4Te_6$) is widely used for this purpose.[46–49] Recently, researchers have explored new types of cryogenic materials that can be very useful for power generation in aerospace applications. Iron antimonide ($FeSb_2$) showed very large power factor (below 100 K) as compared to other developed TE materials in this temperature range.[50–53] Near-room temperature and up to 500 K, chalcogenides are the best-known TE materials. Bismuth telluride (Bi_2Te_3) based materials are mainly investigated for ambient temperature applications and they have shown very decent performance with n- and p-type dopants.[44] At present, TE modules fabricated from n-type Bi_2Te_3 and p-type $Bi_{2-x}Sb_xTe_3$have exhibited conversion efficiencies up to 4 -5 %.[54,55]

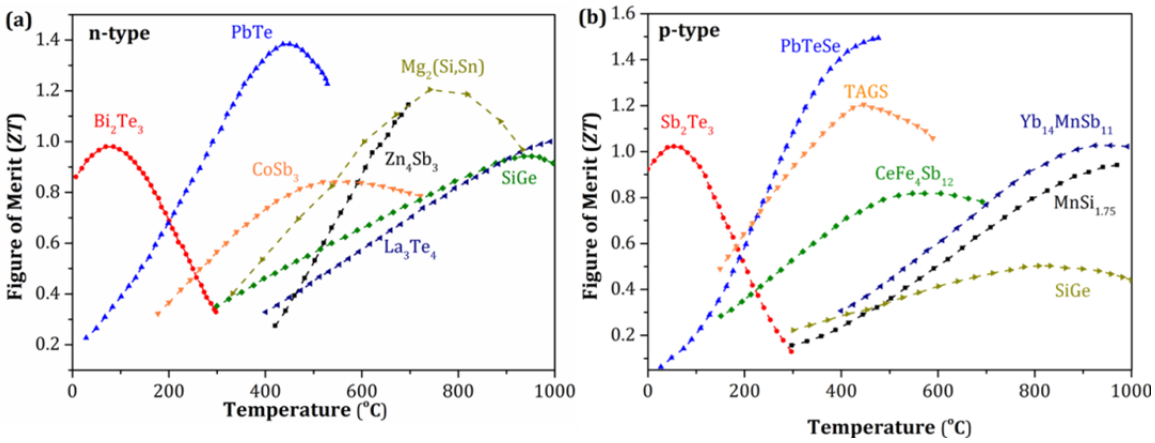

Figure 1.6 *ZT versus temperature in bulk TE materials; (a) n-Type, (b) p-Type* [17]

In the middle temperature range from 500 to 900 K, skutterudites, clathrates, and lead chalcogenides (LAST) have shown the best TE performance.[56–59] Cobalt antimonide ($CoSb_3$) based skutterudites have demonstrated the best *ZT* values in the temperature range of 600 to 800 K.[60–64] However, clathrates and PbTe have shown the best TE performance between 700 and 900 K.[65–69] Comparatively, all of these materials are expensive and their constituents are not earth abundant which led to research to an environment friendly class of TE materials known as silicides.[70] Magnesium silicides (Mg_2Si) as n-type[71,72] and higher manganese silicides ($MnSi_x$) as p-type [73] TE compounds are replacing these middle temperature range applications. Metal oxides (*e.g.* ZnO) [74–77] and half-Heusler intermetallics (*e.g.* HfNiSn) [78–81] are the other class of TE materials, which are favorable at high temperature ranges (above 900 K). Figure 1.6 displays different class of materials with respect to their suitable temperature range for TE applications.[17]

1.3 Strategies for Improving ZT

In 1990s, a renewed interest and novel strategies opened several prospects to enhance the *ZT* values after four decades in TE research. One of the most commonly applied strategies is reducing the lattice thermal conductivity by utilizing different nanoengineering methods.[82]

1.3.1 Nanostructured Bulk Thermoelectrics (TEs)

Research on nanostructured (NS) bulk TEs increased after the publication of *Dresselhaus*' theories of TE materials with superior performances that showed routes to tailor the otherwise interconnected physical parameters of *S*, σ and *κ*.[83] *ZT*

values can be simply enhanced by decoupling the thermal and electrical transport, by introducing some scattering mechanism in NS bulk TEs.[84] Recently, excellent review articles have described in detail the interface nanoengineering in the nanocrystalline bulk TEs.[15] Figure 1.7 presents some developed strategies in NS TE materials to improve the figure of merit.[85–88] These approaches have been suitable in decreasing the κ_{latt} via phonon scattering at the grain boundaries, thus lowering the overall κ.[89] Additionally, the power factor is enhanced and the overall *ZT* can be improved in polycrystalline bulk NS TE materials with high compaction density.

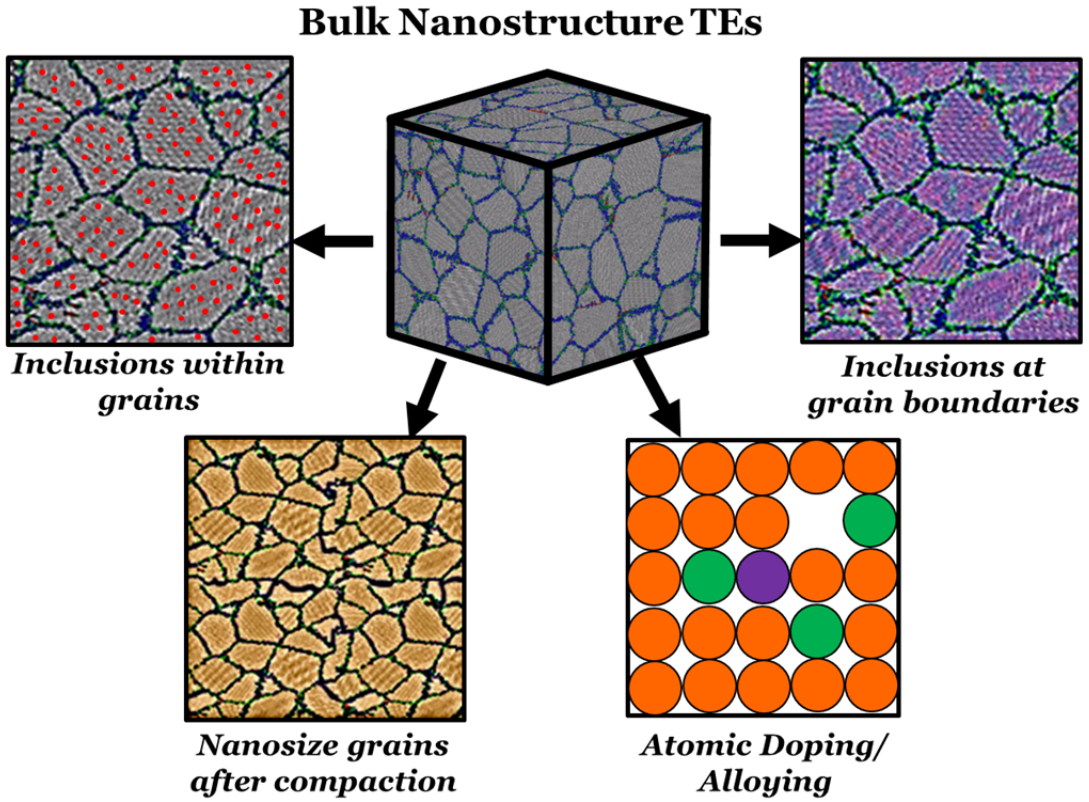

Figure 1.7 *Strategies to improve ZT in Bulk Nanostructured TEs*

1.3.2 Nano-engineered Bulk TEs

A different approach to enhancing the *ZT* values may be the complex structures, such as host-guest structures. Previously, complex structures containing bulk materials such as clathrates, skutterudites, and zintl phases have shown great potential to improve the TE performance.[90–92] Solid solution alloying in these complex structures is another way of improving *ZT.* For instance, by generating a disorder in the unit cell analogous to interstitial sites or partial occupancy in alloys may enhance

the power factor.[93] Recently, optimizing the doping concentration and band gap engineering was carried out to enhance the *ZT*.[25,94] Typically, a good TE material is a heavily doped semiconductor which improves the power factor ($S^2\sigma$) while keeping κ low.[86,95] At most, dopants are carefully selected and limited for different bulk TEs, which causes further limitations of this concept.[96] Unfortunately, the long-term stability of dopants in many TE materials is not investigated in detail. *Toprak et. al.* reported synthesis of doped (Ni and Te) skutterudites, which enhance the overall *ZT* by 30 % via reducing κ by utilizing nanoengineering approaches including nanosized grains and substitution doping of the crystal.[60,62,63]

1.3.3 Nano-composite Bulk TEs

Nanocomposite (NC) may be defined as a class of bulk material that consists of nanosize inclusions (from same type and/or another kind of material) in the matrix and/or at the grain boundaries. Recently, few review articles explained this concept within bulk TEs.[84,86,97,98] In addition, it has been proven experimentally that these heterogeneous systems may display enhanced *ZT*. Mainly, the number of interfaces increased in NC as compared to bulk material which caused κ_{latt} to decrease without interfering significantly with σ. Actually, electrical carriers consider a path of least resistance with lower resistivity through this NC like-structure, which is known as the percolation effect. However, phonons are confronting with obstacles and scattered extensively at the grain boundaries, which result in the reduction of overall κ. A NC can be fabricated from nanomaterials while preserving nanostructure during processing. Carrier transport in such complex systems is not well established as compared to phonon transport. Although theoretical explanations of these concepts are being investigated, there are many experimental results reporting an improvement in *ZT*.[61,99–102] In our earlier work, some examples of nanocomposites have shown improved TE performance due to the grain boundary pinning of skutterudites by zirconia nanoparticles.[61,103]

1.4 TE Materials Synthesis

Synthesis method of TE material is of the utmost importance, as it requires appropriate optimization of critical parameters to obtain defect free crystal, desired microstructure, accurate stoichiometry and high purity TE materials. Currently,

available TE materials can be prepared by a variety of physical and chemical processes that produce nanosized bulk materials in powder or solid ingot form. These methods can be classified under two categories as “top-down” and “bottom-up” approaches. However, preparing TE materials with nano-scale grain size distribution is often challenging with these methods due to thermodynamics and kinetics of the reactions.[104]

1.4.1 Top-Down Approach

In this approach, micro and/or macro scale materials are broken down to nano-scale domains. Solid-state synthesis followed by mechanical alloying and melt alloying routes are commonly applied methods utilized in top-down approaches. Solid-state synthesis and melting techniques are well known from metallurgical processes where a stoichiometric ratio of high purity elemental components (in powder or compacted form) are heated or melted for long durations to obtain the desired TE phase. Conversely, in mechanical alloying, pure elemental micron size powders are ball milled for many hours to obtain submicron or nanoscale bulk TE materials.[105]

1.4.2 Bottom-Up Approach

Chemical fabrication routes are mainly bottom-up approaches that can allow a more desirable control over the particle size and morphology of a TE material through fine-tuning of various parameters. The role of chemical synthesis and their effect on the TE properties of nanomaterials can be explored through the comparison of TE performance. Solvothermal, hydrothermal, solution co-precipitation, sol gel, micro emulsion, and electrochemical synthesis are well known bottom-up approaches.[9] Solution co-precipitation and solvothermal chemical reactions can produce various TE materials with improved TE performance. Chemical precursor used in these reactions is less expensive as compared to the materials in their pure elemental form. In our earlier works, we have obtained pure phase of nanostructured TE materials in large quantities. However, due to some technical and kinetic limitations it is not possible to produce all types of TE materials via bottom-up synthesis.

1.5 Representative high-performance TE materials

In this thesis, we have investigated the following materials to improve the TE performance via nano-structuring and nano-composite formation methodologies.

1.5.1 Chalcogenides based Alloys

The onset of chalcogenides was introduced in the 1950s. Moreover, they have been vastly investigated as a TE material for low temperature applications (300-450 K). Bismuth telluride (Bi_2Te_3) is the major type of chalcogenides in the TE market. Nevertheless, this material became of great interest after *Poudel et. al.*, reported that NS bulk Bi_2Te_3 doped with antimony (Sb) showed a *ZT* of 1.4 at 373 K. Subsequently, $Bi_{2-x}Sb_xTe_3$ was fabricated via mechanical alloying (ball milling) followed by consolidation using a hot press. Microstructural evaluation describes the high *ZT* values that were attributed to the decrease in *κ*. Later, studies showed about 20% increase in *ZT* by introducing silicon carbide (SiC) nanoparticles as inclusions at the grain boundaries. The addition of SiC enhanced the power factor, also reduced the thermal conductivity because of the grain boundary pinning effect.[106] Recently, *Zhao et. al.* introduced the percolation effect to tune the TE transport properties.[107] They obtained two different sizes of Bi_2Te_3 (and then mixed with different ratios) and after compaction an enhanced *ZT* value was observed with an optimized fine/coarse volume ration of 6/4. However, reproducibility and repeatability of these results are still important open questions for all TE research groups because most of the composites are not performing as measured and reported earlier. TE evaluation results deviate significantly and thus self-doping and reliability of measurements exhibit issues in these materials.

1.5.2 Silicide based Alloys

Silicides based TE alloys were first proposed by *Niktin* in 1958, and recent nanostructuring concepts have revived the silicides TE research. Among all types of TE materials, silicides are the most environment friendly, inexpensive, earth abundant, and excellent oxidation resistant materials at high temperatures. Currently, silicide based TE materials are considered to be the best candidate for power generation application in mid- to high temperature range (400-800 K). Magnesium silcide (Mg_2Si) and their solid solutions (with Sn or Ge) are promising n-type materials. Higher manganese silicides ($MnSi_x$) are known to be the best p-type candidates due to their unique layered crystal structure and anisotropic properties. Recently, many groups have reported improved *ZT* values of 1 for Mg_2Si doped with Bi at 800 K.[108] Similarly, manganese silicides' (HMS) TE performance improved up to 50 % through nanostructuring.[109] Few research groups have also demonstrated

power generation device (TEGs) made of n-type Mg_2Si (Sn doped) and p-type HMS.[110,111] Although silicides showed major developments recently, some other challenges may impede further improvement.

1.5.3 Iron Antimonide ($FeSb_2$)

Recently, iron antimonide ($FeSb_2$) has been investigated as it has demonstrated high Seebeck coefficient and electrical conductivity at far below ambient temperatures (10-100 K).[112,113] This can be considered as one of the best TE material candidates for low temperature applications, such as in space. Very few reports have been published on the TE performance of $FeSb_2$ and their alloys. Synthesis of nanostructured $FeSb_2$ is a challenge using top-down approaches that is why it is limited to only bottom up synthesis. *Nolas et. al.* established chemical synthesis routes for nanosized $FeSb_2$ followed by SPS compaction to obtain the desired phase. They have reported two times improved Seebeck coefficient at 50 K and the resistivity also decreased from 500 to 400 mΩ-cm below 50 K.[50,114] In another work, *Kieslich et. al.* reported thermal conductivity of $FeSb_2$ suppressed around 80 % as compared to the bulk value, which was due to the grain boundary scattering of phonons on the nanoscale.[115]

1.6 Objectives

The objective of this thesis is to develop effective NS TE materials via application of nanoengineering strategies. Main focus is the synthesis of nanomaterials via bottom-up and/or top-down approaches and preserving the nanostructure during compaction process. The overall goal is to produce n- and p-type NS TE material with improved figure of merit, *ZT*.

Briefly, the specific objectives are as follow:

1. Fabrication of chalcogenides based materials via cost effective chemical synthesis to obtain nanomaterials. Specifically:
    a. Nanostructured n-type Bi_2Te_3 via solution co-precipitation and thermochemical treatment
    b. Nanostructured p-type Sb_2Te_3 via solution co-precipitation and fast chemical reduction

2. Optimization of critical SPS parameters (such as sintering temperature, applied pressure, holding time and heating rates) for chalcogenides while consolidating these materials to preserve the nanostructure, to reduce thermal conductivity.
3. Bottom-up chemical synthesis and detailed characterization of $FeSb_2$ for low temperature TE applications.
4. Fabrication of silicide based TE materials through mechanical alloying (top-down approach). Specifically:
    a. n-type Mg_2Si by ball milling for an optimized reaction time and followed by materials' characterizations to identify the phase of the materials.
    b. Doping of Al and Bi in n-type Mg_2Si nanomaterials and to investigate its effect on TE performance.
    c. Fabrication of p-type HMS via ball milling by utilizing optimized reaction time followed by detailed physiochemical characterizations.
    d. Study the effect of ytterbium (Yb) as nanoinclusions/grain boundary pinning in HMS matrix
5. Optimization of SPS critical parameters (such as sintering temperature, applied pressure, holding time and heating rates) while consolidating these materials to preserve the nanostructure and obtain the desired phases.

Chapter 2

2 Experimental Methods

2.1 Materials Synthesis

In this thesis, two different synthesis methods were utilized to fabricate the NS TE materials. Chalcogenides based TE materials were prepared by a chemical synthesis referred to as the bottom-up approach, and Silicide based materials were synthesized by the top-down approach, which is referred to as mechanical alloying (MA).

2.1.1 Chemical Synthesis of Chalcogenides

Bismuth telluride (Bi_2Te_3) and antimony telluride (Sb_2Te_3) are well-known n- and p-type chalcogenide TE materials, respectively. Fabrication of these materials via bottom-up methods have been scarcely reported.[116–118] However, their synthesis methods require high temperature process for an extended duration involving organic solvents and the batch size per experiment is quite limited, therefore, this process is not practically applicable for TE industry. We are presenting an alternative strategy to prepare Bi_2Te_3 and Sb_2Te_3 via solution chemical synthesis as detailed below.

2.1.1.1 Synthesis of Bismuth Telluride (Bi_2Te_3) Paper I

Bi_2Te_3 was prepared via chemical solution based on the co-precipitation technique. Thermodynamic [44] modeling was performed to identify the desired pH value to obtain precipitates of the required phase. Stoichiometric ratio of bismuth nitrate pentahydrate ($Bi(NO_3)_3.5H_2O$) and tellurium oxide (TeO_2) metal salts were prepared in nitric acid solution. Sodium hydroxide (NaOH) solution was used as a precipitating agent. Both solutions were mixed in a reactor and as-prepared cloudy white precipitates were filtered off and washed with deionized (DI) water several times to remove the by-products and unreacted precursors. Precipitates were dried at 80 ^oC overnight. The dried powder was further thermally treated at a calcination temperature of 250 ^oC to obtain the oxide phases of elements, and further underwent hydrogen (95%) reduction of Bi and Te oxides at 400 ^oC. After 2 hours, the reduction yielded the final desired phase of Bi_2Te_3. Figure 2.1 schematically shows the flow diagram of the synthesis of Bi_2Te_3.[119,120]

2.1.1.2 Synthesis of Antimony Telluride (Sb_2Te_3) Paper II

Sb_2Te_3 was also prepared by the co-precipitation route and the same steps were followed as detailed in 2.1.1.1. Stoichiometric ratio of antimony trichloride ($SbCl_3$) and tellurium oxide (TeO_2) were dissolved in nitric acid (HNO_3, 3M); sodium hydroxide (NaOH, 3M) was used as the precipitating agent which resulted in off-white oxide precipitates. The precipitates were washed many times to remove the byproducts followed by drying at 80 ^oC overnight in a vacuum oven. The dried precipitates of antimony oxide (Sb_2O_3) and tellurium oxide (TeO_2) were reduced by utilizing sodium borohydride ($NaBH_4$). Hydrogen (H_2) was produced from $NaBH_4$ and reacted with oxide precipitates of Sb and Te to convert the product into final phase. During the reduction reaction, a reflux system was accompanied with a three-neck flask to prevent the violent release of H_2 gas. The mixture was left for 12 hours to complete the reduction reaction of oxide precipitates.[121] Figure 2.1 presents the synthesis flow chart for chalcogenides nanomaterials.

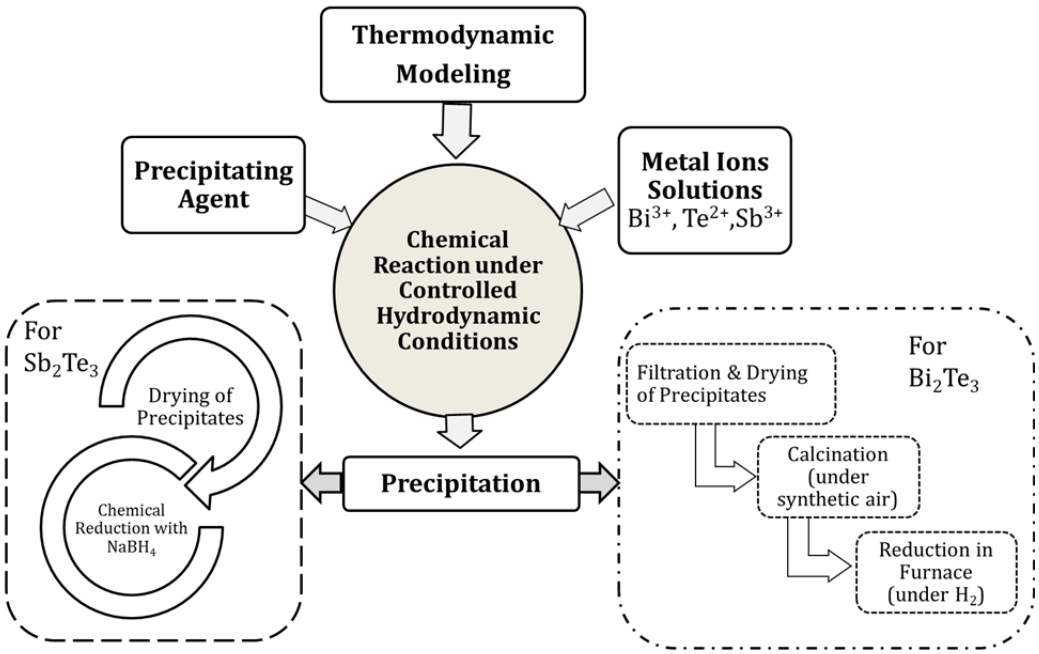

Figure 2.1 Flow chart of chemical synthesis of Chalcogenides

2.1.1.3 Synthesis of Iron Antimonide ($FeSb_2$) Paper V

$FeSb_2$ nanopowder was produced by using a template and a surfactant free chemical synthesis. Iron (III) nitrate ($Fe(NO_3)_3.6H_2O$) and antimony (III) acetate ($Sb(CH_3COO)_3$) with 99.995% purity were purchased from Sigma Aldrich. Stoichiometric proportions of Fe and Sb respective metal salts (1:2) were mixed and melted in hexane (50ml) at 60 ^oC. At 48 ^oC, $Fe(NO_3)_3.6H_2O$ melts and can be added to $Sb(CH_3COO)_3$ to subsequently form a homogenous mixture. After heating for 2 hours, the mixture was cooled to room temperature. Excess solvent was removed and the prepared precursor was dried at 60 ^oC in a vacuum oven for 12 hours. The dried sample was crushed and calcination was performed at 250 ^oC to produce the oxide phases of Fe and Sb. The final desired phase of $FeSb_2$ was obtained after hydrogen (5% H_2 with 95 %N_2) reduction in a tube furnace at 350 ^oC with a heating rate of 2 ^oC/min for 2 hours of dwelling time.

2.1.2 Mechanical Alloying of Silicides

Mechanical alloying (MA) is a top-down approach and recently applied by many researchers for TE material synthesis. The alloy is formed as a result of the solid phase reaction of pure elements, which is performed by mechanical impact during high energy ball milling.[73,122] MA has a great advantage in the formation of various alloys although; it is difficult to prepare via any other synthesis method. It is

very important to optimize the reaction conditions in order to obtain materials with a high purity and desired crystal phase.[123] Silicide based n- and p-type TE materials were prepared by MA and the details are given below. Figure 2.2 presents the flow diagram of fabrication steps involved in the silicide material synthesis.

2.1.2.1 Synthesis of Magnesium Silicide

NS magnesium silicide (Mg_2Si) was prepared from commercially available high purity (99.999 %) pieces of Mg_2Si. The raw material was converted to a powder in a planetary ball milling setup for 8 to 24 hours with an optimized rotational speed of 330 rpm in the presence of hexane and argon (Ar) gases. Doping elements (such as Bi and Al) were also introduced initially to prepare different compositions of silicide alloys. Metal oxide inclusions were introduced during the milling procedure to achieve homogenous mixing of the composites.[72]

2.1.2.2 Synthesis of Higher Manganese Silicide

Higher manganese silicide (HMS) with nominal composition of $MnSi_{1.73}$ was prepared using the ball milling setup for 8 hours with a rotation speed of 330 to 400 rpm. Hexane and Ar was used during the milling process. Similarly, other alloys of HMS were prepared by adding individual elements with its' stoichiometric ratio to obtain the final phase. NC samples were prepared by adding Yb during the MA step.

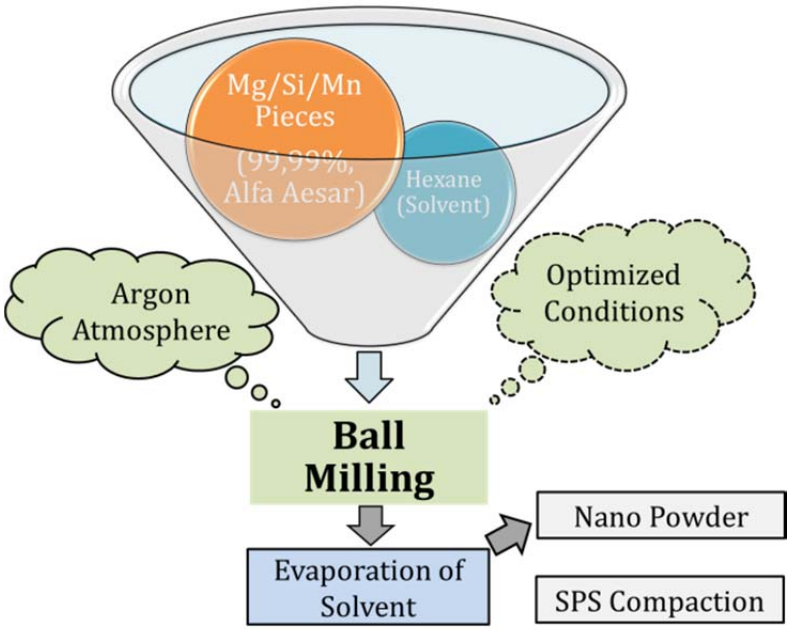

Figure 2.2 Synthesis of Silicide TE materials

2.2 Spark Plasma Sintering (SPS)

SPS is a rapid sintering technique, which has been successfully demonstrated for the compaction of ceramics, intermetallic and semiconductors while preserving the nanostructure. SPS has received great attention due to the short sintering temperatures and electric pulse heating in the conducting samples. In addition, SPS can attain better microstructure and high compaction densities in a short period of compaction process.

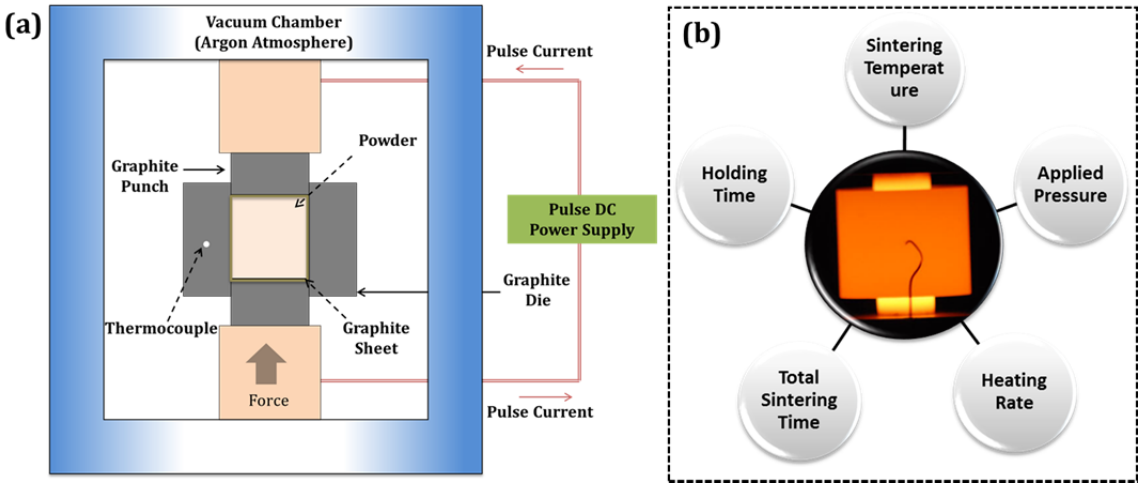

Figure 2.3 *Spark Plasma Sintering; (a) Setup, (b) Important parameters*

An electric discharge, or DC pulse, is passed through the graphite die and the conducting sample, which generates localized temperature within the sample for sintering. Heating rate and sintering temperature can be altered while changing the capacity and quantity of DC pulses. SPS can sinter materials ranging from a few hundred to 2000 ^{o}C and the pressure can be varied from 2 kN to 20 kN. Different size of dies can be used for compaction. Figure 2.3 presents a schematic of SPS setup and compaction experiments used for preparing samples.

2.2.1 Optimizations of SPS Parameters

There are few critical SPS parameters (as shown in figure 2.3 (b)), which are essential for the optimization of consolidation conditions for each material type. Generally, SPS process depends upon sintering temperature, applied pressure, heating rate, holding time and total sintering time. Heating rate and sintering temperature can be adjusted by tuning the DC pulse strength and applied time. Similarly, applied pressure can be selected depending upon the type of material.[73,124]

2.2.1.1 SPS Optimization of Chalcogenides

SPS conditions such as sintering temperature, applied pressure and holding time were optimized for chalcogenides samples. Bi_2Te_3 was used to screen SPS parameters to achieve high compaction density while preserving nanosize grains. Sb_2Te_3 sample was compacted at similar SPS conditions.[125]

2.2.1.2 SPS Optimization of Silicides

Silicides were investigated for different SPS parameters to attain the desired phases in HMS (p-type) and the preservation of the nanostructures in Mg_2Si (n-type). Furthermore, fabrication of silicide alloys such as doping of Bi and Al in Mg_2Si systems and grain boundary pinning with metal/metal oxide powders to form nanocomposites were succeeded by SPS. HMS samples were studied in detail to observe the proper phase formation after the solid-state reactions of Mn and Si. [72,73,123]

2.3 Characterizations

2.3.1 Crystal Structure Characterization

X-ray diffraction (XRD) studies were performed on nanopowders and SPS compacted samples to identify the crystalline phases. Philips X'pert Pro and PW3710 diffractometer were used with Bragg-Brentano geometry and Cu K alpha source of 1.54 Å wavelength. Rietveld refinement of XRD patterns was exploited to determine the crystallite size, lattice parameters and quantitative analysis of different crystal phases.

2.3.2 Microstructure Characterization

Scanning electron microscopy (SEM) was performed to visualize the morphology and size of the nanoparticles and grains. Dried nanopowder and fractured surfaces of SPS compacted samples were prepared on carbon tape. Images were obtained via Zeiss FEG-SEM Ultra 55 and Sigma Zeiss FE-SEM. Energy dispersive x-ray spectroscopy (EDX) was executed with the aid of Oxford X-Max EDX detector. Transmission electron microscopy (TEM) was performed using a JEOL FEG-JEM 2100F system. TEM samples were prepared on carbon coated copper grids by drying the drop casted sample suspension. Hexane or ethanol was used to disperse the nanoparticles. SPS compacted sample was crushed and dispersed in a solvent to prepare TEM samples. Selected area electron diffraction (SAED) was also utilized to investigate the

crystallinity of individual grains. Focused Ion Beam SEM (FIB-SEM) was used to prepare TEM samples for high-resolution TEM and EDX analysis.

2.3.3 Thermal Characterization

Thermal gravimetric analysis (TGA) was used to evaluate the thermal behavior of as-precipitated precursors with the aid of TGA-Q500 from TA instruments. TGA was used to determine calcination and reduction temperature of some investigated samples.

2.3.4 TE Transport Characterization

Paper 1: TE evaluations are performed to determine the figure of merit. Bi_2Te_3 samples were measured at German Aerospace Center (DLR), Germany within the temperature range of 325-475 K. S and σ were measured simultaneously and a temperature gradient was applied while the setup and procedure are described elsewhere.[62] Thermal diffusivity of Bi_2Te_3 samples was evaluated by laser flash apparatus, Netzsch LFA 427 and heat capacity was measured by differential scanning calorimeter (DSC). Moreover, κ was calculated from the product of the thermal diffusivity, Cp and density. Details of these measurements are also cited in an earlier work.[126]

Paper 2 and 5: Sb_2Te_3 samples were tested at Fraunhofer-IPM, Germany by using an in-house built *ZT* meter. S, σ and κ parameters were measured; simultaneously, SPS compacted sample was cut into required dimensions (5x5x5 mm^3). Anisotropic behavior of Sb_2Te_3 samples was also measured in parallel and perpendicular directions to the sintering. Details of the measurement setup are given in *Jacqout et. al.*[127]

Paper 3-4 & 6-9: TE characterizations of silicide based materials were established at Italian National Research Institute-CNR, Italy. S and electrical resistivity (ρ) was measured in Ar atmosphere from RT to 600 ^oC with help of in-house built setup, which was calibrated with NIST standards. Details of the setup and measurements are elaborated in earlier published work.[128] Thermal diffusivity and Cp was measured from LFA and DSC respectively, followed by calculating κ by the product of Cp, thermal diffusivity and density.[128]

Chapter 3

3 Results and Discussions

This section is divided into three classes of materials as chalcogenides (Bi_2Te_3 and Sb_2Te_3 based compounds) for ambient temperature, iron antimonide ($FeSb_2$ compound) for low temperature, and silicides (Mg_2Si and HMS based compounds) for intermediate temperature region. Each section summarizes the results from appended papers, see relevant paper for further details.

3.1 Chalcogenide Based Materials

Bi_2Te_3 and Sb_2Te_3 based chalcogenides were investigated: We demonstrated easily scalable bottom-up chemical synthesis route for these materials. We can control grain size with nanoengineered processing approaches, which is done very little in the TE industry. In the following sections, details of fabrication and investigation of nanosized Bi_2Te_3 and Sb_2Te_3 are presented.

3.1.1 n-type Chalcogenides (Paper I)

Bismuth telluride (Bi_2Te_3) was synthesized via a chemical solution based co-precipitation method. Chemical equilibrium simulation from Medusa software [44] shows the desired pH value to obtain an intimately mixed phase of precipitates. For Bi_2Te_3 precursor a pH value of 2 is selected. Calcination temperature was identified from thermal gravimetric analysis (TGA) in synthetic air condition on dried precipitates. TGA under Hydrogen gas (5 % H_2 and 95 %N_2) flow was conducted to identify the reduction

temperature and the reaction heating rate. According to the TGA observations, calcination was performed at 250 ^{o}C for 2 hours and reduction reaction was carried out at 400 ^{o}C for 3 hours. Up to 20-30 grams of nanostructured Bi_2Te_3 was successfully produced with a yield of ca. 90 percent. This method can develop smaller particles with plate like morphology as compared to the earlier reported method.[129] SEM analysis of calcined and reduced powder was performed to study the morphology and particle size. Reduced Bi_2Te_3 shows plate like morphology with an average particle size about 80 nm and thickness of the plates are in the range of 5-10 nm, as shown in Figure 3.1 (a). EDX analysis confirms Bi to Te atomic ratio (2:3) in the reduced sample and no oxides were detected in the final product.

Figure 3.1 (b) presents XRD patterns from calcined and reduced nanopowders. XRD analysis after calcination reveals only Bi_2O_3 and TeO_2 phases as indexed with JCPDS number 27-0050 and JCPDS number 01-0870, respectively. However, XRD results from reduced sample confirmed pure Bi_2Te_3 rhombohedral crystal structure, which is indexed with JCPDS number 85-0439. Crystallite size of reduced nanopowder calculated by Scherrer equation is roughly 50 nm.

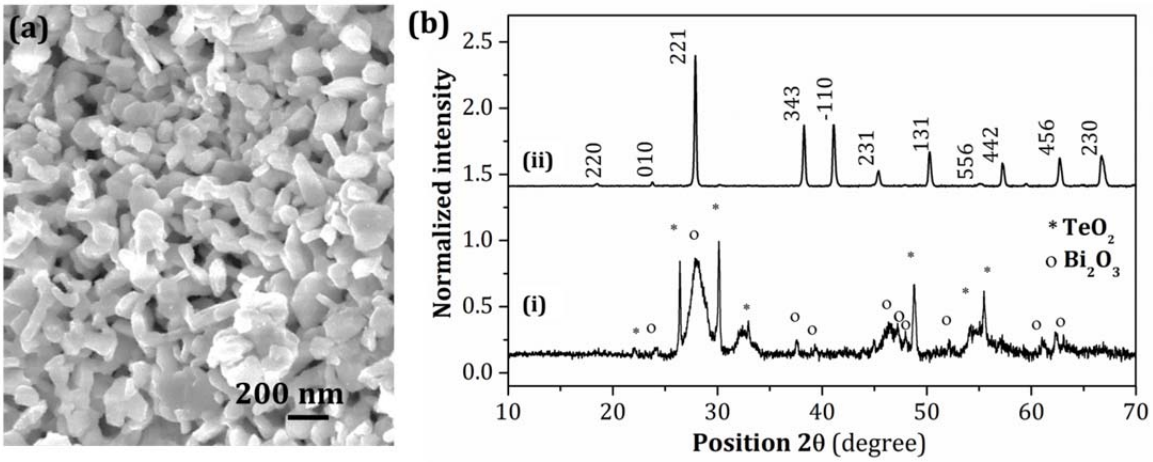

Figure 3.1 *Physiochemical characterizations of Bi_2Te_3; (a) SEM of reduced nanopowder, and (b) XRD analysis of Calcined (i) & (ii) Reduced samples.*

SPS critical parameters were studied to achieve highly dense pellets with nanostructured grains. Most of the samples could achieve more than 95 % compaction density while grain size increased from 80 nm to 380 nm. Details of SPS conditions and experiments are reported in the appended paper I. Figure 3.2 displays micrographs from fractured surface of Bi_2Te_3 SPS samples at 0 minute holding time and 4 minutes holding time. It can be observed that 723 K sintering temperature with 4 minutes holding time

has increased the grain size to roughly 400 nm as compared to 723 K with 0 minute holding achieved grain size around 300 nm. Similarly 648 K with 0 minute holding time shows less densification but 4 minutes holding time increases the grain size. Thus holding time for Bi_2Te_3 samples may achieve very high compaction densities but also causes the grain growth, which is not profitable for TE transport properties. A sample compacted at 673 K with 0 minute holding time was selected for the TE evaluations. XRD analysis on compacted samples at 673 K with 0, 2 and 4 minutes holding time showed pure Bi_2Te_3 phase.

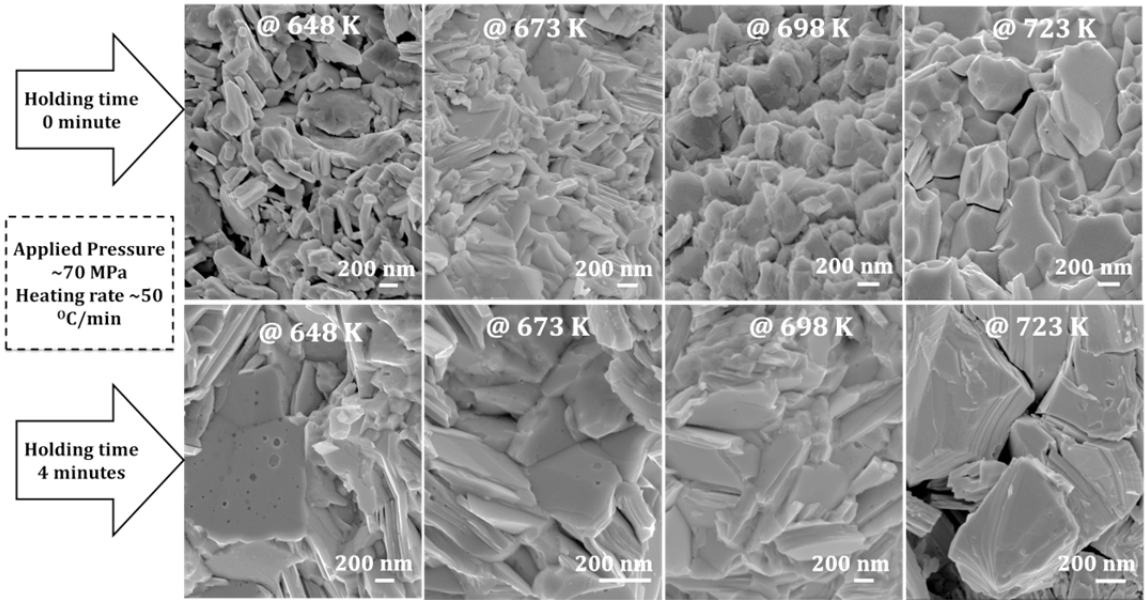

Figure 3.2 *SEM micrographs from fractured surface of SPS samples.*

Figure 3.3 (a & b) display TEM analysis on SPS sample compacted at 673 K with 0 minute holding time, whereas inset in Figure 3.3 (a) presents a selected area diffraction pattern (SAED). Results confirmed polycrystallinity of the sample while inter-atomic distance (d) values were measured with the help of image J software[130,131] and the reported results are in agreement with XRD analysis.

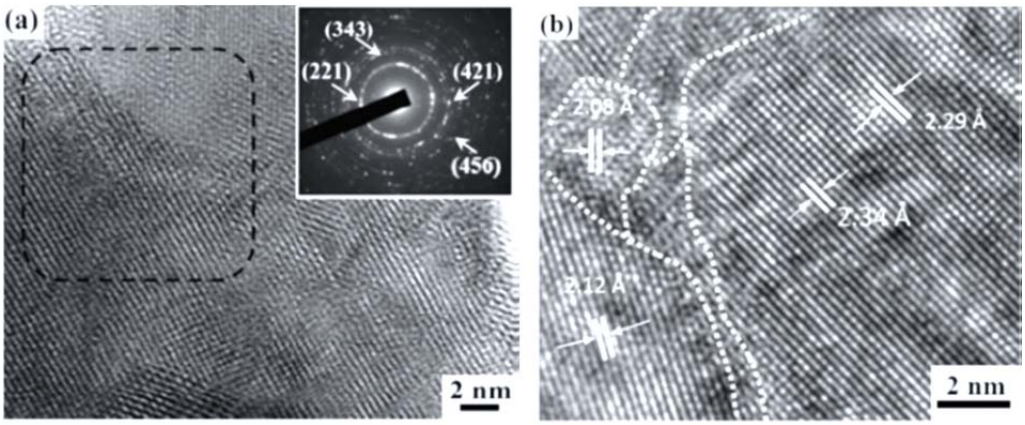

Figure 3.3 *SPS Bi_2Te_3 sample; (a) TEM Analysis (SAED pattern inset), (b) HRTEM.*

TE transport property evaluation revealed negative S values, which confirms the n-type behavior of Bi_2Te_3 sample. S value of -120 µV/K at 325 K is slightly higher as compared to that reported by *M. Scheele et. al.* [132] Enhancement in S is mainly attributed to preferential scattering of low energy carriers at the grain boundaries. Figure 3.4 (a & b) presents σ, κ and *ZT* in the temperature range of 325-450 K. Highest σ value about 2000 S/cm was obtained around 300 K, however it decreases with an increase in temperature, which is a typical semi-metallic character. This sample showed around 50% higher σ values at 300 K, as compared to the previous state of the art undoped Bi_2Te_3. Total κ obtained is around 0.8 W/mK @ 350 K and results are comparable to that reported by *Yu et. al.*[133] We achieved a *ZT* of around 1.1 at 340 K, which is higher than the previous record at the respective temperature range.[133]

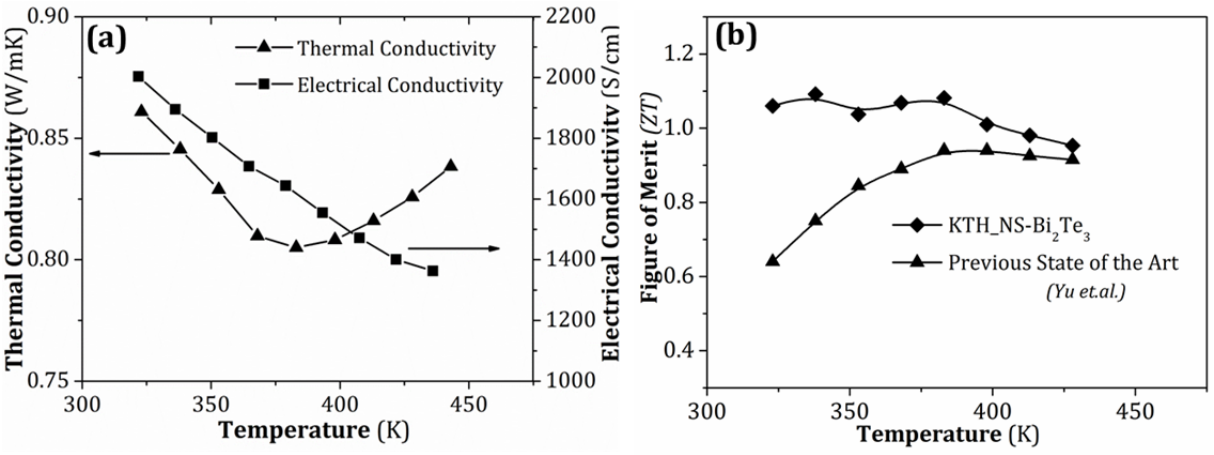

Figure 3.4 *TE transport evaluations of Bi_2Te_3; (a) Electrical conductivity & Thermal conductivity, and (b) Figure of merit, ZT.*

3.1.2 p-type Chalcogenides (Paper II)

Nanopowder of antimony telluride (Sb_2Te_3) was produced via a chemical solution route. This synthesis route has decreased the number reaction steps that are favorable and

economical for industrial scale production. As-prepared Sb_2Te_3 particles were analyzed by SEM and EDX for particle/grain size, morphology and chemical composition. EDX confirms the stoichiometric compound with desired ratio of Sb to Te (2:3). SEM micrographs from as-prepared nanoparticles show the particle size is roughly 50 to 200 nm, while grain size grows after the SPS process, as can be observed in Figure 3.6 (b) obtained from fractured surface of SPS sample.

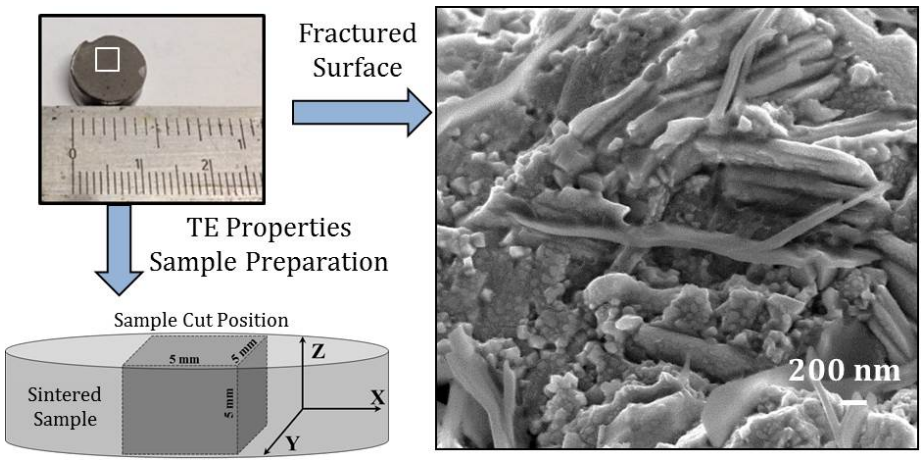

Figure 3.5 *Schematic of sample cut for TE measurements and SEM micrographs from Sb_2Te_3 compacted samples*

XRD analysis from as-prepared nanopowder and SPS samples has shown rhombohedral Sb_2Te_3 crystal structure. Crystallite size for as-prepared sample is about 40 nm but after SPS it rose to 90 nm. Anisotropy of Sb_2Te_3 samples were measured with the help of *ZT* meter constructed by IPM-Fraunhofer. A sample with 5*5*5 mm^3 was cut from the pellet as shown in Figure 3.5 and the evaluation was performed along and perpendicular to the direction of compaction.

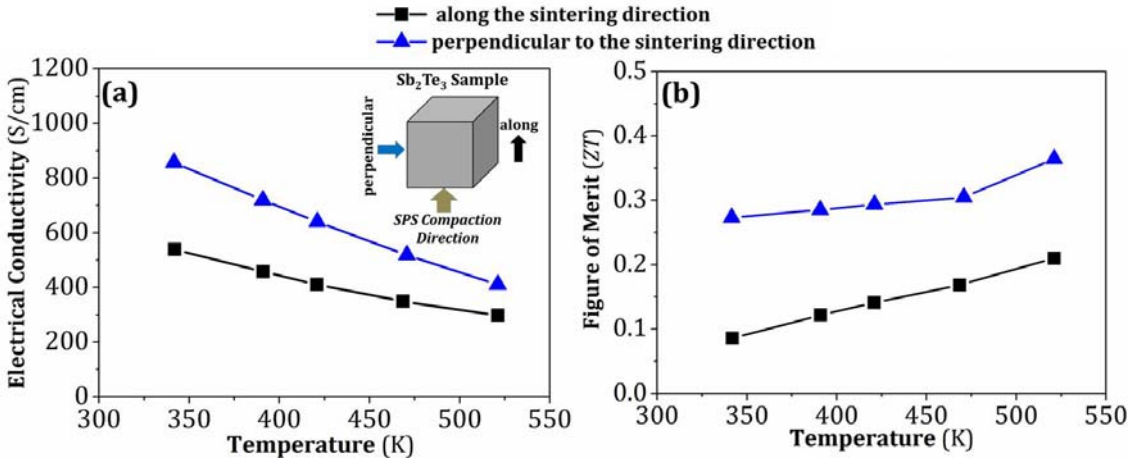

Figure 3.6 *Anisotropy TE characterizations of Sb_2Te_3; (a) Electrical Conductivity, and (b) Figure of Merit*

Positive Seebeck coefficient confirms its p-type nature. Along the SPS direction, S value is below 100 μV/K while it reaches a maximum value of 150 μV/K @ 525 K in perpendicular measurements. Similar enhancement was observed in electrical conductivity measurements. Sample along the sintering direction displays lower σ values, below 600 S/cm while increased to 1000 S/cm at 350 K for perpendicular measurements. It confirms the strong anisotropy in the Sb_2Te_3 sample. However, κ values exhibit similar results for both the directions (1.2 – 1.5 W/m.K), which may be due to extensive growth of the grains. TE figure of merit enhanced due to the electrical anisotropic characteristics and highest *ZT* value 0.35 at 525 K was observed in perpendicular measured sample and results are displayed in Figure 3.6 (b).

3.2 $FeSb_2$ based Material (Paper III)

Iron antimonide ($FeSb_2$) was prepared for the first time via a novel bottom-up chemical synthesis method. Metal salt melting route can produce large amount of samples per batch. Also our process is faster as compared to recently published reports.[50,51] SPS was carried out at 400 ^oC for 2 minutes holding time and 70 MPa, these conditions were derived from our chalcogenides work. SEM micrograph from reduced nanopowder and SPS fractured surface are shown in Figure 3.7 (a & b).

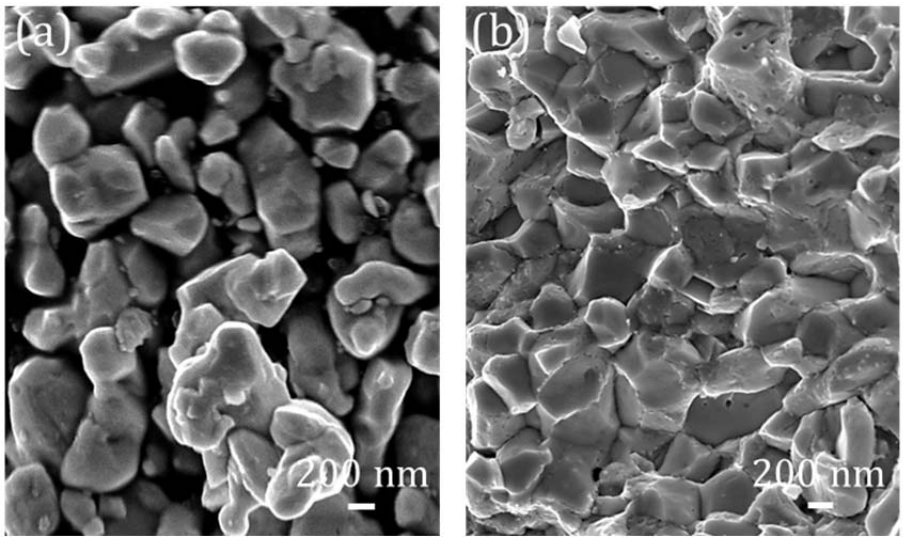

Figure 3.7 *SEM micrographs of $FeSb_2$ sample; (a) As-prepared, (b) Fractured SPS*

It is clearly observed that as-prepared particles are widely distributed from 100 to 400 nm and compacted sample preserved the nanostructure. SEM-EDX results did not show any impurity of oxides, which confirms our sample's purity, is better than samples reported in the literature.[50,51]

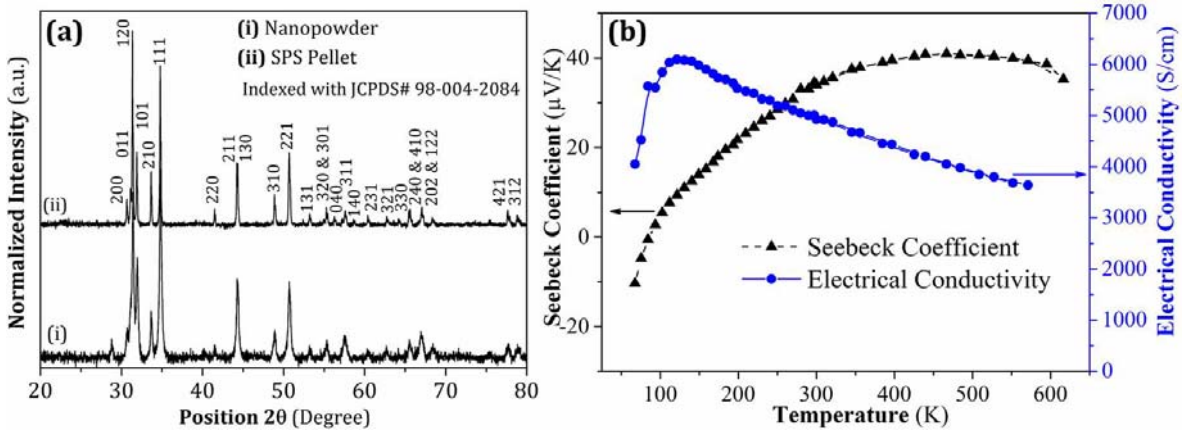

Figure 3.8 *$FeSb_2$ Sample; (a) XRD patterns from Nanopowder and SPS pellet, and (b) TE transport Properties (Seebeck Coefficient and Electrical Conductivity)*

XRD analysis revealed the pure $FeSb_2$ crystal phase and diffraction pattern from as-prepared powder and SPS sample are shown in Figure 3.8 (a). The small impurity XRD peak belonging to Sb at 29 degrees in the as-prepared nanopowders, dissolved homogenously in the matrix after SPS pellet formation. All XRD peaks were indexed with the reference pattern JCPDS number 98-004-2084. Figure 3.8 (b) shows TE transport properties measured from 50 to 600 K. All samples were measured twice while heating up and cooling down. $FeSb_2$ show very small S values and interestingly, it has shown n-type conduction below 100 K while p-type conduction after 100 K. However, σ values in our samples are rather high and it is almost three times higher than those reported in previous reports.[51,114] κ was measured only from 300 to 600K and a maximum value of 7.14 W/mK was obtained, which is comparable to bulk crystals of $FeSb_2$. Overall *ZT* above 300 K was calculated and maximum value of 0.04 at 600 K was observed. These results show 10 times improved *ZT* values as compared to *Nolas et. al.*[114] which could be achieved only due to enormous increase in electrical conductivity.

3.3 Silicides based Materials

Recently, silicide materials have attained great attention due to their mid to high *temperature power generation application. They are also well known due to their low*-cost, high reliability, high earth abundance and environment friendly characteristics. Solid solutions of magnesium silicide (Mg_2Si) and higher manganese silicide ($MnSi_x$) are proven n- and p-type promising candidates for TE applications. In this thesis we focus on the synthesis and processing of nanoengineered silicides with improved TE performance.

3.3.1 n-type Silicides (Paper IV)

Nanopowder of Mg_2Si was prepared by utilizing the ball milling method followed by compaction using optimized SPS conditions. SEM micrograph and the particle size analysis from ball milled (BM) powder are shown in Figure 3.9 (a & b). SEM reveals irregular shape of the BM particles; a mixture of small and large aggregates. Particle size was calculated by image J, software and histogram in Figure 3.9 (b) displays the distribution of particle size. Average particle size is roughly 230 nm and 60 % of the particles are below 300 nm. EDX confirms 5 to 7 % of magnesium oxide (MgO) phase as impurity in the BM sample and mapping analysis shows small grains of MgO dispersed in the whole matrix.

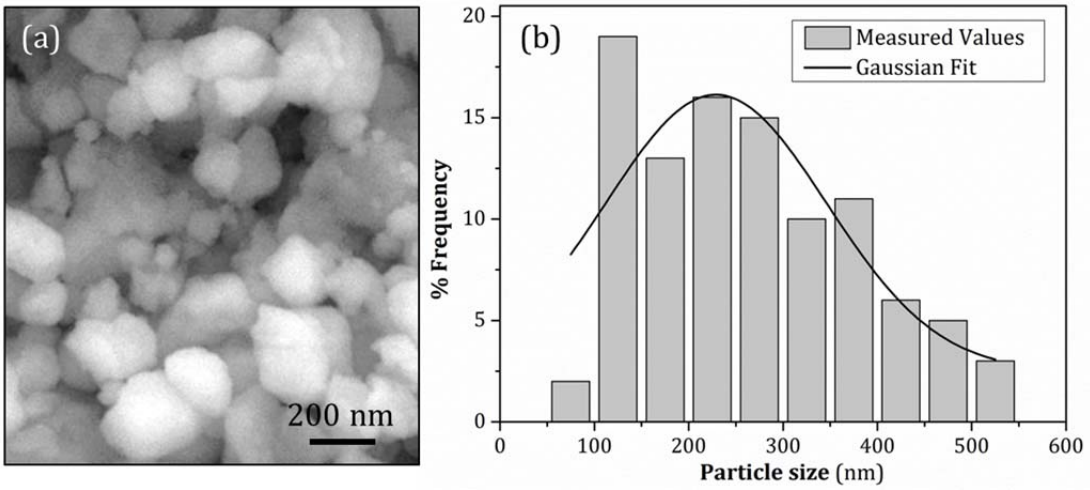

Figure 3.9 *(a) SEM micrograph, (b) Particle size analysis for BM Mg_2Si sample*

TEM and SAED analysis was carried out to determine nanoparticles phase purity. TEM confirms the particle size in the range 200 - 300 nm and SAED pattern reveals mixture phase of MgO and Mg_2Si. Dark and bright field imaging was also performed. A series of SPS experiments were carried out to achieve the highest compaction density while preserving the nanosize grains. Three different sintering temperatures and holding time was employed in order to screen the SPS parameters. However, the heating rate and applied pressure were kept constant in all experiments. Samples compacted at 650 ^oC obtained poor densification (below 85 %), whereas samples sintered at 750 ^oC and 850 ^oC showed densification more than 92 %. Table 3.1 explains the compaction densities and average crystallite size from three samples and further details of SPS experiments are published in appended paper IV. XRD patterns were analyzed by Rietveld refinement with the help of Maud program, to determine crystal structure, crystallite size and quantitative analysis of the existing crystal phases.

Table 3.1 *Optimization of SPS Parameters of BM Mg_2Si*

Sample ID	SPS Parameters			Relative Density (g/cm^3)	Theoretical Density (g/cm^3)	Compaction Density (%)	Average Crystallite Size (nm)
	Temperature (^oC)	Pressure (KN)	Holding Time (min)				
MS_02	750	8.8	5	2.01	2.19	91.5	150
MS_04	750	8.8	2	2.11	2.19	96.2	150
MS_06	750	8.8	0	2.13	2.13	97.2	240

Samples sintered at 750 ^{o}C with holding time 0, 2 and 5 minutes were used to perform the TE transport evaluation. All samples display n-type behavior, since S values are negative and vary in the range of -200 to -475 μV/K from room temperature up to 600 ^{o}C. Figure 3.10 (a) displays electrical resistivity (ρ), however SPS sample compacted at 750 ^{o}C with 2 minutes holding time demonstrated two times lower ρ values compared to the SPS sample with 5 minutes holding time (up to 100 ^{o}C). S and ρ results are in good agreement with published reports on undoped Mg_2Si.[134,135] Total κ reaches a high value of 12 W/mK, which decreases with increasing temperature, and finally reaching the lowest value of about 4.5 W/mK in all samples. These results are better than bulk undoped Mg_2Si and comparable to that reported by other research groups.[136] Figure 3.10 (b) displays the *ZT* results, although no visible trend in *ZT* values with respect to sintering holding time was observed.

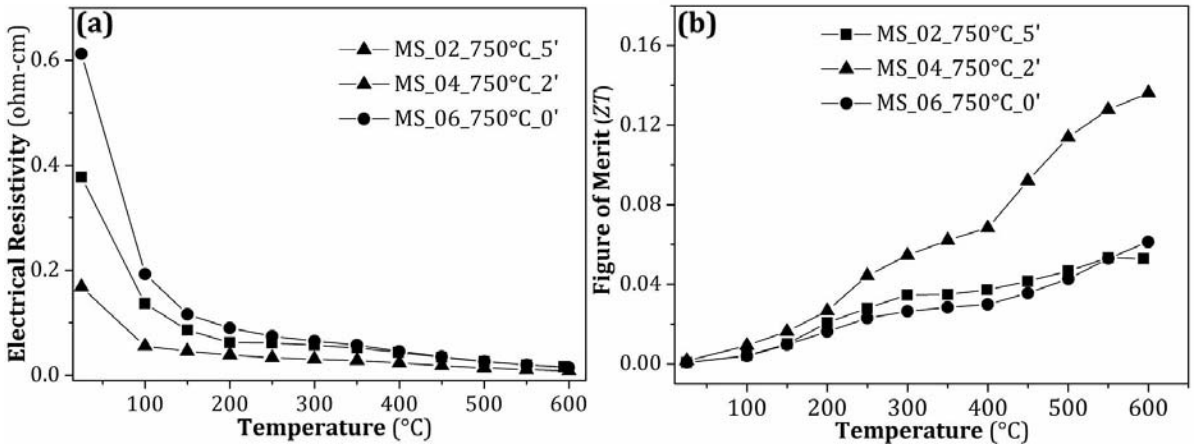

Figure 3.10 *TE transport evaluations of undoped Mg_2Si; (a) Electrical Resistivity, and (b) Figure of merit.*

3.3.1.1 Al-Doped Mg_2Si (Paper V)

Many reports have demonstrated enhancement in the TE performance of Mg_2Si solid solutions with doping on Mg and/or Si atomic sites. We utilized aluminum (Al) as dopant and four differently doped samples with x=0.005, 0.01, 0.02, and 0.04 were prepared,

whereas x is the Al:Mg_2Si molar ratio. Optimized SPS conditions on undoped Mg_2Si were utilized from paper IV. Details of synthesis and characterization are given in the appended paper V. XRD patterns of undoped and doped samples are shown in Figure 3.11 (a); results reveal slight impurity of MgO (about 6 %) which is derived from the raw material as reported in our earlier work.[137] Crystallite size calculated from Rietveld refinement analysis is about 100 to 140 nm. SEM and EDX showed uniform distribution of Al in the Mg_2Si matrix, however, oxide of Mg was observed as confirmed by XRD. Detailed temperature dependent TE transport properties of undoped and Al doped Mg_2Si samples are presented in appended paper V. ρ decreased with increasing temperature, however, effect of Al doping can be observed with decreasing ρ values at high Al content. S values are negative which reveal n-type conduction and the results present lower S values as compared to the literature.[138] This reduction in S values are mainly attributed due to more MgO content in these samples.[137] All samples have shown predominant contribution of κ_{latt}. Al doping did not reduce the thermal conductivity but it improved the electrical properties, which enhanced the *ZT* value from 0.1 to 0.55 at 600 ^{o}C as displayed in Figure 3.11 (b). These results are comparable to earlier reported work.[138]

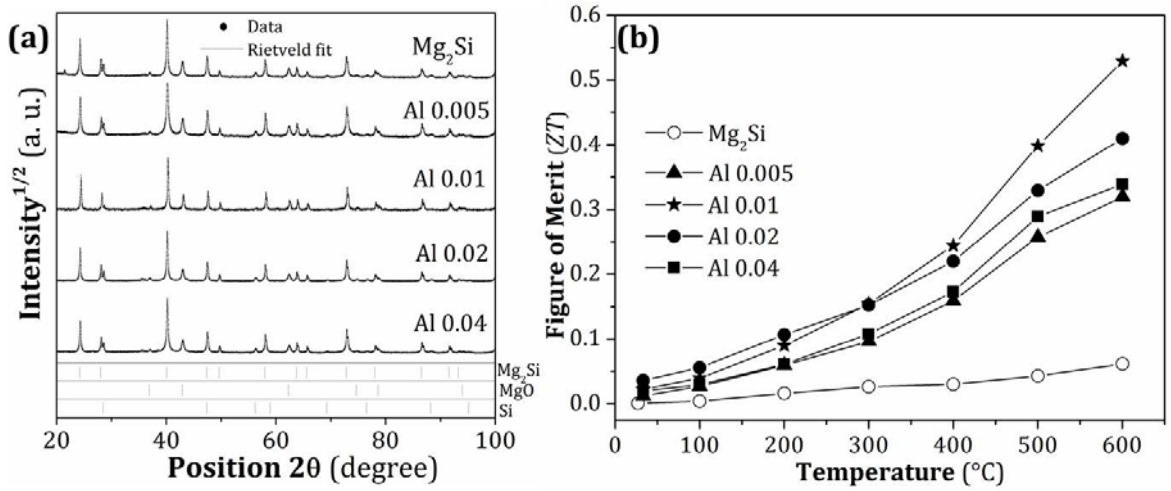

Figure 3.11 *Al-doped Mg_2Si; (a) XRD Patterns, (b) Figure of merit.*

3.3.1.2 Bi doped Mg_2Si (Paper VI)

Bismuth (Bi) was selected as dopant to enhance the TE performance of n-type silicides. All samples were prepared with similar protocols as mentioned in appended paper IV and V. Three different concentrations of Bi to Mg_2Si (x=0.010, 0.015 and 0.020) were chosen for doping experiments. XRD analysis revealed that Mg_2Si is the major crystalline phase and some free Bi was detected in the bulk sample. However, MgO content in these

samples is roughly 5 %, which has been controlled during the SPS process. Moreover, detailed XRD studies reveal two types of Mg_2Si phases with different cell parameters. The ratio of latter doped phase increases with the increase of Bi content. However, former doped phase is essential for better mechanical and TE transport properties. Thus, Bi doping in Mg_2Si is inhomogeneous and this might occur due to poor diffusion of Bi in the grains. Details are described in the appended paper VI. SEM analysis reveals that the grains are in the range of 200 to 400 nm.

Table 3.2 *Carrier Concentration of Bi-doped Mg_2Si Samples*

Sample	. Phys. Lett. tration (*10^{19} cm^3)	Mobility (cm^2/Vs)
X=0	0.50	205
X=0.010	3.16	31.3
X=0.015	3.56	28.7
X=0.020	4.14	32.7

Hall measurements at room temperature were used to measure the carrier concentration and mobility in all samples, and results are summarized in Table 3.2. Reported values are lower than earlier reports,[139]which is mainly due to incomplete doping of Mg_2Si. Figure 3.12 (a) presents the *ZT* values of undoped and Bi doped Mg_2Si. All doped samples have higher *ZT* values as compared to undoped sample. We have achieved a highest *ZT* value 0.8 at 600 ^oC, which is comparable to the earlier reports.[139]

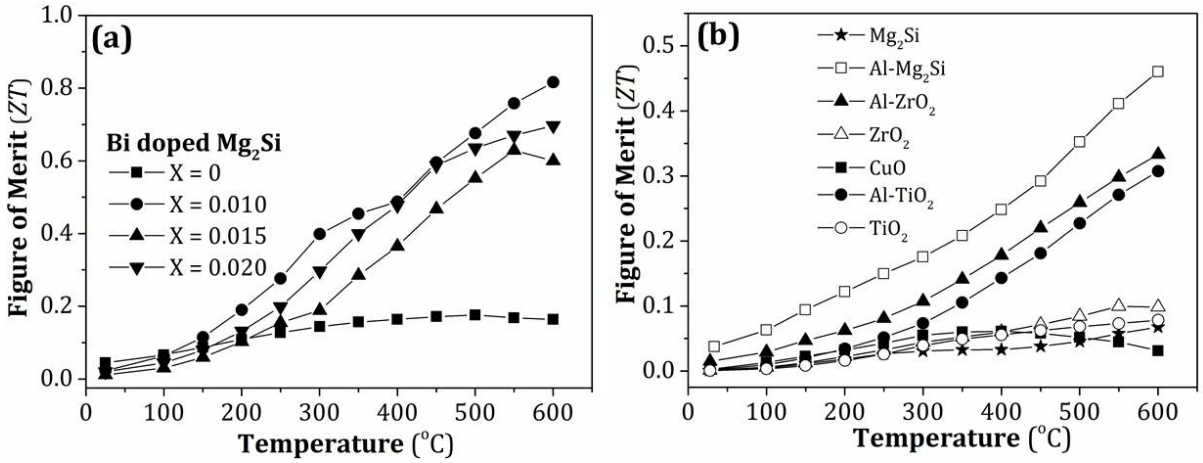

Figure 3.12 *TE Figure of merit; (a) Bi doped Mg_2Si, (b) Metal oxide and Mg_2Si composites*

3.3.1.3 Metal oxides and Mg_2Si Nanocomposites (Paper VII)

Nanocomposites (NC) introduce grain boundary pinning to reduce the total κ and overall increase in *ZT*. NC was fabricated with different metal oxide (TiO_2, ZrO_2, and CuO) particles in undoped Mg_2Si and 2 at % Al doped Mg_2Si nanopowder. Al-doped sample was selected because it showed decent *ZT* values at 600 ^oC as reported in our earlier work.[71] Details of metal oxide nanoparticles and SPS compaction parameters are presented in appended paper VII. Al-doped Mg_2Si showed no free Al in the XRD pattern, with only 2 % of MgO content, however, metal oxide nanopowders results new phase formations such as $TiSi_2$, $ZrSi_2$ and Cu_3Mg_2Si. Back scattered electron diffraction (EBSD) images were obtained from the fractured surface of SPS samples. SPS samples of Mg_2Si NC showed Ti, Zr and Cu rich grains from TiO_2, ZrO_2 and CuO respectively. EDX revealed Ti, Cu, Zr and Al over the whole matrix of the sample. Figure 3.12 (b) displays *ZT* results from various Mg_2Si NC; it can be observed that most of the metal oxide composites could not improve the performance, which is mainly due to the inhomogeneous mixing and metallic phase formations in Mg_2Si NC.

3.3.2 p-type Silicides (Paper VIII)

HMS is known as the best p-type candidate for TE silicides and $MnSi_x$ (x=1.71-1.75) are the most favorable compounds for TE materials. In this work we have selected $MnSi_{1.73}$ composition for investigation. HMS was fabricated by ball milling of elemental Mn and Si powder obtained from Alfa Aesar with 99.95 % purity. As-prepared powders were compacted at 750 to 1000 ^oC under 50 to 90 MPa applied pressure with 5 to 10 minutes holding time. SPS samples were analyzed in XRD, SEM and EDX to determine the crystal purity, grain size and chemical composition respectively. All the results are presented in appended paper VIII. XRD pattern from BM sample showed no solid-state reaction between Mn and Si. However, all SPS pellets reveal tetragonal $MnSi_{1.73}$ as major crystal phase and cubic MnSi as impurity crystal phase. In the recent literature, MnSi phase was identified as metallic character which may reduce the TE transport performance.[140,141] HMS phases content increased upto 95 % with the increase of sintering temperature from 750 to 1000 ^oC and applied pressure from 50 to 90 MPa. Microstructure of compacted samples were observed in EBSD images; samples compacted at 1000 ^oC showed larger grain size as compared to the sample compacted at 900 ^oC. Phase stability of the compacted samples was checked by TGA and DSC experiments. Results did not show any degradation of the compacted sample after two

sequential DSC cyclic runs as reported in appended paper VIII.[142] Samples compacted at 800, 900 and 1000 °C with 90 MPa applied pressure and 5 minutes holding time were selected for TE transport evaluation. S and ρ increase with increasing temperature, however, sample compacted at 800 °C have higher resistivity than the one compacted at 1000 °C. It is mainly due to different compaction density of these samples.

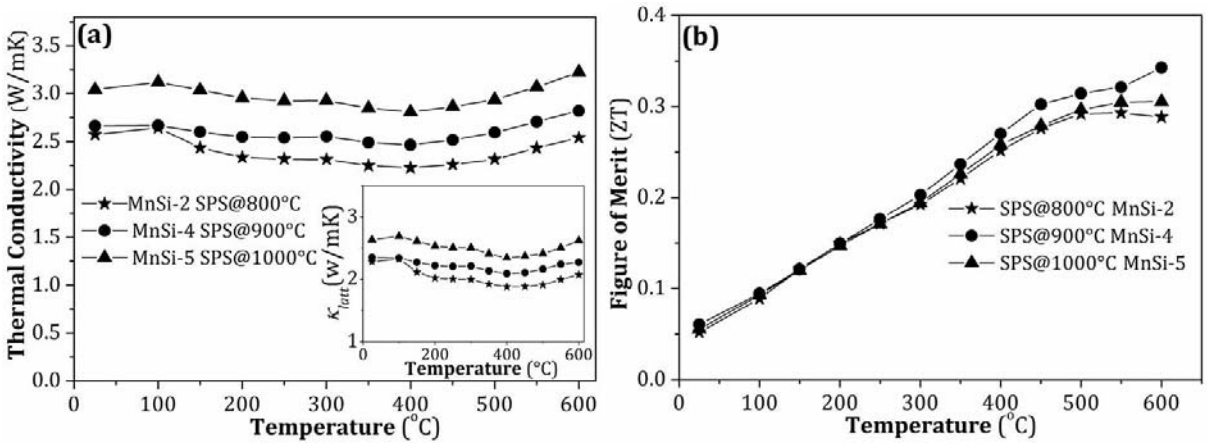

Figure 3.13 *TE transport evaluation of HMS; (a) Thermal conductivity and (b) Figure of merit.*

Figure 3.13 (a) displays similar observation that low compaction density sample (in SPS@800 °C MnSi-2) attributed to lower total κ and vice versa. However, inset in Figure 3.13 (a) proves that κ_{latt} is the major contributor to total κ and our results are comparable with those reported by *Itoh et. al.*[143] MnSi-4 sample showed the highest *ZT*, of 0.34 at 600 °C, among the three samples. This is due to slightly higher S values as compared to the other two samples. This is mainly attributed to the lower MnSi phase in this sample. Comparable *ZT* values are reported in the literature as well.[143]

3.3.2.1 Yb and HMS Nanocomposites (Paper IX)

Ytterbium (Yb), as rare earth metal inclusions was used to prepare the HMS NC.A stoichiometric ratio of Si to Mn: 1.73 was selected with two different concentrations (0.5 wt % and 1.0 wt %) of Yb metal. As-prepared particles were consolidated at 950 °C, 5 minutes holding time, and 75 MPa applied pressure. XRD patterns revealed no signals of Yb in BM sample and very small amount of HMS phase was manufactured. Under SPS solid-state reaction, HMS and MnSi phases were formed as shown in XRD patterns obtained from SPS samples. SEM-EDX mapping analysis was performed to investigate the Yb inclusions in SPS samples. Most of the Yb grains allocated at the boundaries of large grains. HRTEM image confirms the presence of different phases and Yb grains as

shown in Figure 3.14 (a). Line profile TEM-EDX analysis was carried out to determine the composition of nanocomposite and results are displayed in Figure 3.14 (b). Yb can be observed at the grain boundaries as shown in line profile (iii) in the graph.

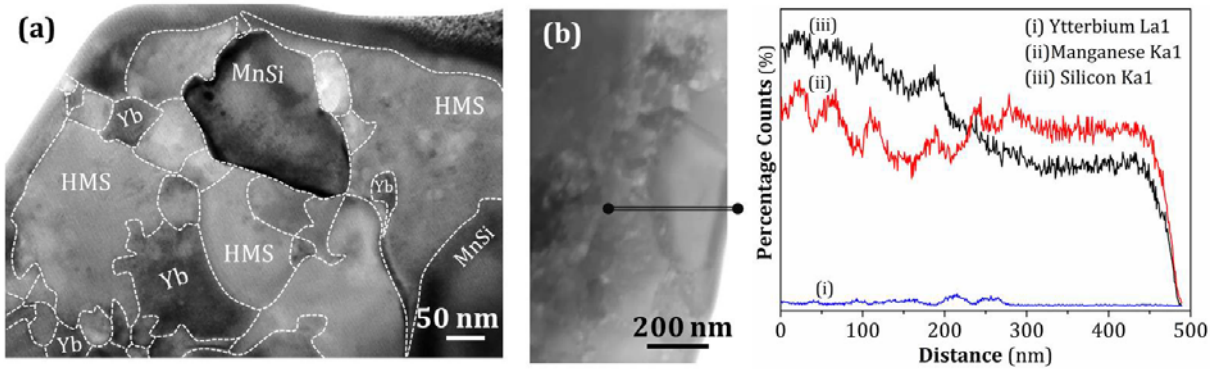

Figure 3.14 *(a) HRTEM image, and (b) TEM-EDX line profile of HMS+Yb 1.0% sample.*

Measurement results from *S* and *ρ* show increase in values with increasing temperature, which correspond to degenerate semiconductor characteristics. Similar observations were reported in earlier literature.[109] All S values are positive, which exhibit p-type conduction behavior. S increased from 150 to 190 μV/K as Yb content increased, similar to predictions of *Norouzzadeh's* for NC.[109] However, *ρ* is strongly influenced from the Yb content, such as *ρ* is roughly half of the pure HMS sample as shown in the figure 3.15 (a). Total *κ* reached higher values as compared to earlier reports,[141] which is mainly due to high amount of cubic MnSi phase. However, Yb HMS NC samples showed reduction in total *κ*, which confirms the success of grain boundary pinning in our samples.

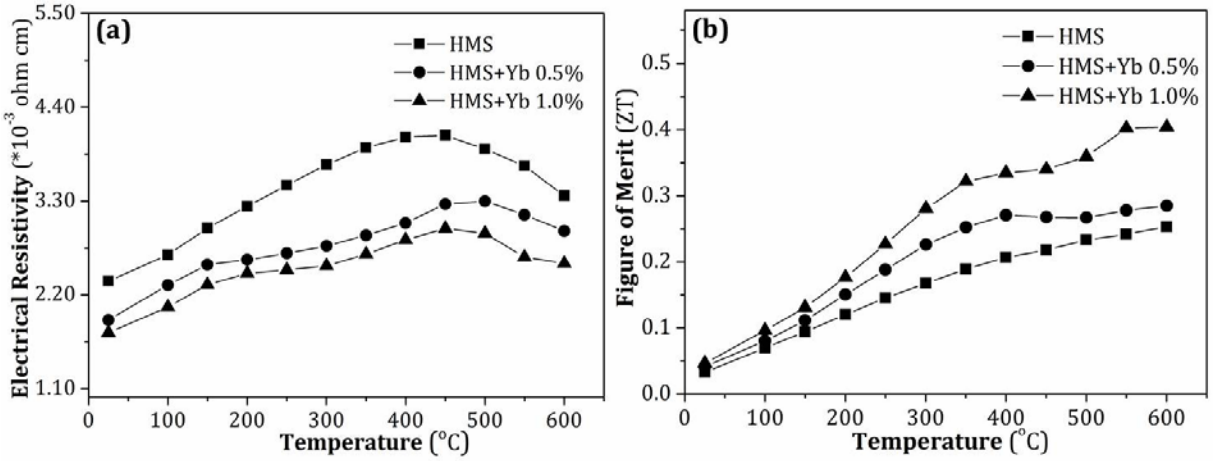

Figure 3.15 *TE transport Evaluation of Yb-HMS NC; (a) Electrical Resistivity and (b) Figure of merit.*

Figure 3.15 (b) displays calculated *ZT* values from pure HMS and their Yb NC. *ZT* value as high as 0.42@ 600 ^{o}C was obtained from the NC with 1.0% Yb content, which is due to the significant decrease in ρ values due to the presence of Yb. In this work, we have successfully demonstrated the fabrication of HMS NC and improved TE performance.

Chapter 4

4 Conclusions

In this thesis, we have utilized various nanoengineering approaches to improve the transport properties of investigated TE materials. Nanomaterials were successfully produced via chemical bottom-up synthesis as well as mechanical alloying techniques. SPS allowed us to achieve very high compaction density and to preserve the nano-grain size. Compacted bulk pellets of different TE materials showed enhanced TE performance, which may offer opportunities for their use in various applications in the industry.

Solution based chemical bottom-up synthesis was used to fabricate the chalcogenides based TE materials (Bi_2Te_3 and Sb_2Te_3), which were successfully prepared in large batches with uniform structure and homogenous compositions. Fine plate like morphology of Bi_2Te_3 was obtained after reduction. SPS optimization on reduced Bi_2Te_3samples yielded 97 % densification with marginal increase in grain size. TE transport properties showed n-type behavior with improved performance, due to enhancement in S and σ values while the power factor was raised 30 %. The ZT of about 1.1 at 340 K was achieved, which is higher than the previous state of the art results [133] on bulk undoped Bi_2Te_3samples.

Sb_2Te_3 was prepared via a similar co-precipitation method except the thermal treatments were replaced with solution chemical reduction with sodium borohydride.

Sb_2Te_3 nanopowder was compacted by SPS with previous optimized conditions. Anisotropic TE transport evaluations were performed in plane and cross plane directions to the compaction direction. Evaluation of *S* and *σ* showed strong anisotropic behavior of Sb_2Te_3 pellets. However, similar *κ* values were observed in both directions, which confirm no effect of thermal properties due to anisotropy. *ZT* enhanced in perpendicular direction to the sintering, which is mainly attributed due increased *S* and *σ* values.

Nanostructured low temperature TE material, $FeSb_2$, was prepared with the help of a novel solution chemical process by melting metal salts of respective chemicals at lower temperatures in an inert liquid media. Melted precursor was thermochemically treated to obtain the final desired phase. A compaction density of 95 % was obtained while preserving the nanostructure. TE transport properties showed enhanced *S* and *σ*, which led to a rather high power factor. Although *κ* was not reduced overall *ZT* values were enhanced due to the gigantic increase in *σ*.

Silicide based n- and p-type TE materials were investigated using nanoengineering methodologies. All silicide TE materials were prepared via top-down approaches by ball milling of source materials to final desired product. The highest *ZT* value achieved in undoped Mg_2Si was about 0.14 at 600 ^oC. In order to increase the TE performance, doping of Al and Bi was utilized on Mg_2Si samples. Al doped Mg_2Si with three different concentrations (x=0.005, 0.01, 0.02, 0.04) showed promising TE performance. A maximum *ZT* value of 0.50 was obtained in Al 0.01 sample, which is mainly due to the decrease in *ρ* values as compared to all other samples. Due to high MgO content it is difficult to observe any effect in decreasing *κ* values. Bi-Doped Mg_2Si samples showed the best *ZT* values around 0.8 at 600 ^oC. Furthermore, metal oxide composites with undoped and Al-doped Mg_2Si samples have demonstrated the grain boundary pinning behavior. TiO_2, ZrO_2 and CuO nanopowders have formed secondary phases such as $TiSi_2$, $ZrSi_2$, and Cu_3Mg_2Si respectively. The Al-doped Mg_2Si with TiO_2 nanoparticles have shown the highest *ZT* value 0.45 at 600 ^oC among all these samples.

HMS has been reported as the best p-type silicide material for TE applications. $MnSi_{1.73}$ prepared via ball milling and as-prepared powder was used to optimize the SPS conditions. Results showed different amount of HMS phases and compaction densities

on 800 ^{o}C to 1000 ^{o}C sintered sample. However, the grains also grew dramatically at 1000 ^{o}C while the compaction density was the highest. HMS synthesis and compaction simultaneously is a big advantage in our studies, which could save enormous amount of energy in the industrial scale production. *ZT* value as high as 0.34 at 600 ^{o}C was obtained. In order to improve the performance of p-type silicide TE materials, HMS nanocomposites with Yb metal inclusions were prepared and demonstrated successfully. TE properties showed slight increase in *ZT* value in 1 % Yb HMS NC. Detailed TEM and EDX analysis revealed the presence of Yb grains in SPS pellets at the grain boundaries.

In summary, bulk nanostructured TE materials were successfully fabricated and characterized with various methodologies. Moreover, the preparation of TE nanostructures via chemical synthesis routes has been demonstrated as powerful tool for the industrial scale production. Improved performance of n- and p-type TE materials provoked by nanostructuring/nano-engineering and optimized compaction by SPS method. However, this is mainly due to the increase of power factor and reduction of thermal conductivity. Most of the TE materials prepared during this thesis work have shown some improvements in *ZT* values.

Chapter 5

5 Future Work

Antimony doped bismuth telluride ($Bi_{2-x}Sb_xTe_3$) is a p-type chalcogenides with improved figure of merit according to several reports with *ZT* of 1 to 1.5. Our solution-based co-precipitation method can achieve nanoparticles of $Bi_{2-x}Sb_xTe_3$compounds, which can be scalable for industrial scale production. Similarly, selenium doped bismuth telluride ($Bi_2Te_{3-x}Se_x$) can be prepared via this bottom-up approach. This may further improve the TE transport properties of n-type chalcogenides. Large batches of n-and p-type have been produced to make the TE power generation device from nanostructured chalcogenides and the concept of the device will be tested in our lab with the compacts made from these samples. $FeSb_2$ with different dopants will be prepared in order to improve the TE performance.

Silicide based materials have shown some oxide impurities in the final product which will be further reduced to obtain the pure form of raw material. Further work will be carried out to improve control of the composition of the samples and the distribution of the secondary phases in the Mg_2Si matrix, which is pivotal for improvement of the thermoelectric performance by decreasing the thermal conductivity. For this purpose, SPS processing will be performed in the current state of the art SPS machine, coupled with gloves box. It is newly installed in SPS National Center established at Stockholm University, Sweden. Handling of powder prepared in the gloves box and continued

compacting in the inert atmosphere may reduce oxide impurities in our samples, which may further improve the TE performance. Single leg silicide based TE device is under construction and will be tested for the power generation applications.

Acknowledgements

This doctoral thesis might have been an unrealistic dream without the support and contributions from many inspiring individuals that formed a productive environment for me to work in. Therefore, I would like to express my sincere gratitude to all the people who contributed in forming such stimulating atmosphere that helped me over the years to complete my work successfully.

First, I would like to express my deepest gratitude to my principle supervisor Assoc. Prof. Muhammet S. Toprak for providing me the opportunity to pursue my PhD degree in the fascinating field of materials for energy related projects in Functional Materials Division at KTH Royal Institute of Technology. I am very grateful to your invaluable inspiration, insightful discussions, great enthusiasm, passionate presentation skills, and worthwhile recommendations during my research career at KTH. My deep and sincere gratitude goes to my co-supervisor Prof. Mamoun Muhammed for his constructive criticism, creative vision, intuitive scientific discussions and immense knowledge on the research projects, which made me determined, active and motivated in my work through the right path.

My sincere gratitude goes to senior researcher at FNM, Dr. Abdusalam Uheida for your useful scientific discussions and providing urgent remedy to all management issues in the laboratories. I am indebted to Docent Wubeshet Sahle and Mr. Hans Bergqvist for their support and all technical trainings on microscopy techniques. Thanks are also due to the former and present members of the FNM for assisting me during my PhD studies. I highly appreciate Dr. Shanghua Li, Dr. Jian Qin, Dr. Fei Ye, Dr. Xiaodi Wang, Dr. Abhilash Sugunan, Dr. Andrea Fornara, Dr. Marta Rull, Dr. Carmen Vogt, Dr. Ying Ma, Dr. Krishna Chandar, Dr. Mazhar Yar, Dr. Najmeh Najmoddin, Dr. Adem Ergul, Mr. Sverker Whalberg, Mr. Aleksey Ruditskiy and Dr. Robina Shahid. Acknowledgements are also due to my PhD colleagues Mr. Mohsen Y. Tafti, Mr. M. Noroozi, Ms. Yichen Zhao, Ms. Heba Asem, Ms. Elena Bedogni, Ms. Adrineh Khachotourian, and all master students Amin, Sathya Prakash, Joydip, Raul, Bejan and all others in the group for their kind support.

Terrance, I do not have words to express my friendship as you have inspired me for many venues in our lives. We learned this together that *LIFE IS BEAUTIFUL*. I especially thanks to Dr. Nader Nikkam for his valuable collaboration and research work in

nanofluids. I will not forget to say millions of thanks to my friends in KTH, Dr. M. Usman, Dr. Usman Qadri, Dr. Aftab, Dr. Anna Fucikova, Dr. Ana Lopez, Dr. Benedetto, Anna, Dr. Luigia, Himanshu, Tobias, Katarina, Dr. Wondwosen, Reza, Roodabieh, Reyhaneh, Sophie, Ove, Laura. Thank you all for your support, love, social activities and great time we shared in eating international foods and playing lots of games over the weekends. Dr. Simone, Dr. Stefania, Dr. Alessia, Dr. Fillipo, Dr. Tatsuya, Dr. Stefano, Dr. Monica and all other CNR colleagues, thank you so much for your great collaboration on our silicide works. Our collaborators in department of energy technology at KTH are acknowledged for their valuable collaboration in NanoHex EU FP7 projects.

Last but not least, I would like to express my greatest gratitude to all members of my family, please accept my warmest and deepest gratitude; I dedicate my thesis to you all. AMI JAN! It was not possible without your prayers and ABU JAN; i love you for all of your support during my education. I will acknowledge, my life role model, my elder brother Yaseen Saleemi, without him I would not reach so far, where I am today. Thank you Bhai for everything, I love you from my deep heart. Choti Maa thanks for all delicious foods, Bagi Sadi and Fiji, thanks for all of your support over the skype. My lovely, sensitive and caring wife Asima Saleemi, Thank you so much for standing beside me during my PhD thesis work, I was not able to finish it without your kind support and motivation. Sanna, Saffa, Waiz, Arwa, Abdul-Wahab, Zara, Ibrahim, Ayesha, M. ESA, Aleysha and the one is coming in December, this thesis for you all to make a high goals and excellent achievements for your future life, make us proud my lovely Kids.

The financial support of the EU on FP7th Frame work projects, EC-FP7 NexTec Project for thermoelectric materials (PROJECT NO: 263167) and EC-FP7 NanoHex Project for nanofluids (PROJECT NO: 228882) are greatly appreciated. This work was also funded by the Italian National Research Council—Italian Ministry of Economic Development Agreement ‘‘Ricerca di sistema elettrico nazionale’’ and Swedish Foundation for Strategic Research to the project Scalable Thermoelectric Materials (PROJECT NO:EM11-0002) and Energimyndigheten for the support on silicide based thermoelectric materials (PROJECT NO: 36656-1). Financial support from Gust. Richert Stiftelsen have increased the TE activities in my research work and assisted in the completion of this thesis.

References

1. R. Kelly, *Over Shoot Day 2014, By Footprint Network August 2014 (http://www.footprintnetwork.org/en)* (2014).

2. G. S. A. Nava, V. H. C. Flores, D. L. C. Chávez, R. D. Chavez, N. Scarlat, J. Mahlknecht, J. F. Dallemand, and R. Parra, Renew. Sustain. Energy Rev. **32**, 140 (2014).

3. British Petrolume, *BP Statistical Review of World Energy June 2012 (bp.com/statisticalreview)* (2012), pp. 1–48.

4. F. M. Agugliaro, M. J. S. Muros, F. G. Barroso, A. M. Sánchez, S. Rojo, and C. P. Bañón, Renew. Sustain. Energy Rev. **16**, 3744 (2012).

5. Q. H. Escobedo, F. M. Agugliaro, J. A. G. Parra, and A. Z. Sierra, Renew. Sustain. Energy Rev. **15**, 721 (2011).

6. S. Kalogirou, Prog. Energy Combust. Sci. **30**, 231 (2004).

7. X. Wang and Z. M. Wang, in *Nanoscale Thermoelectr.*, edited by Z. M. Wang, A. Waag, G. Salamo, N. Kishimoto, S. Bellucci, and Y. J. Park, 16th ed. (Springer International, 2014), pp. 31–32.

8. G. Cao, in *Nanostructures Nanomater. Synth. Prop. Appl.* (2004), pp. 406–408.

9. M. S. Toprak, S. Li, and M. Muhammed, in *Modul. Syst. Appl. Thermoelectr.*, edited by D. M. Rowe, 2nd ed. (CRC Press, Boca Raton, FL, 2012), pp. 17–1.

10. M. S. Dresselhaus, T. Koga, X. Sun, S. B. Cronin, K. L. Wang, and G. Chen, in *Int. Conf. Thermoelectr. ICT, Proc.* (1997), pp. 12–20.

11. H. Alam and S. Ramakrishna, Nano Energy **2**, 190 (2013).

12. J. Minnich, M. S. Dresselhaus, Z. F. Ren, and G. Chen, Energy Environ. Sci. **2**, 466 (2009).

13. M. G. Kanatzidis, Chem. Mater. **22**, 648 (2010).

14. D. Zhao and G. Tan, Appl. Therm. Eng. **66**, 15 (2014).

15. M. M. González, O. C. Calero, and P. D. Chao, Renew. Sustain. Energy Rev. **24**, 288 (2013).

16. A. Shakouri, Annu. Rev. Mater. Res. **41**, 399 (2011).

17. G. J. Snyder and E. S. Toberer, Nat. Mater. **7**, 105 (2008).

18. G. G. Yadav, J. a Susoreny, G. Zhang, H. Yang, and Y. Wu, Nanoscale **3**, 3555 (2011).

19. T. M. Tritt, Annu. Rev. Mater. Res. **41**, 433 (2011).

20. B. P. Ball, MRS Bull. Energy Q. **38**, 446 (2013).

21. A. Ioffe, Sci. Am. **199**, 31 (1958).

22. R. C. Chu and R. E. Simons, in *Int. Conf. Thermoelectr. ICT, Proc.* (1999), pp. 270–279.

23. H. J. Goldsmid and G. S. Nolas, in *Int. Conf. Thermoelectr. ICT, Proc.* (2001), pp. 1–6.

24. L. E. Bell, Sci. Mag. **321**, 1457 (2008).

25. G. S. Nolas and J. Poon, MRS Bull. **31**, 199 (2006).

26. M. H. Elsheikh, D. A. Shnawah, M. F. M. Sabri, S. B. M. Said, M. H. Hassan, M. B. A. Bashir, and M. Mohamad, Renew. Sustain. Energy Rev. **30**, 337 (2014).

27. S. B. Riffat and X. Ma, Appl. Therm. Eng. **23**, 913 (2003).

28. M. Kishi, H. Nemoto, T. Hamao, M. Yamamoto, S. Sudou, M. Mandai, and S. Yamamoto, in *18th Int. Conf. Thermoelectr. Proc. ICT* (1999), pp. 301–307.

29. G. Snyder, Electrochem. Soc. Interface **17**, 54 (2008).

30. J. F. Li, W. S. Liu, L. D. Zhao, and M. Zhou, NPG Asia Mater. **2**, 152 (2010).

31. E. Altenkirch, Phys. Zeitschrift **10**, 560 (1909).

32. E. Altenkirch, Phys. Zeitschrift **12**, 920 (1911).

33. H. J. Goldsmid and R. W. Douglas, Br. J. Appl. Phys. **386-390**, (1954).

34. H. Goldsmid and A. Penn, Phys. Lett. A **2**, 7 (1968).

35. D. M. Rowe, V. S. Shukla, and N. Savvides, Nature **290**, 765 (1981).

36. L. D. Hicks, T. C. Harman, and M. S. Dresselhaus, Appl. Phys. Lett. **63**, 3230 (1993).

37. W. Liu, K. C. Lukas, K. McEnaney, S. Lee, Q. Zhang, C. P. Opeil, G. Chen, and Z. Ren, Energy Environ. Sci. **6**, 552 (2013).

38. R. J. Mehta, C. Karthik, B. Singh, R. Teki, T. Borca-Tasciuc, and G. Ramanath, ACS Nano **4**, 5055 (2010).

39. G. S. Nolas, D. T. Morelli, and T. M. Tritt, Annu. Rev. Mater. Sci. **29**, 89 (1999).

40. A. Majumdar, Science **303**, 777 (2004).

41. A. Date, A. Date, C. Dixon, and A. Akbarzadeh, Renew. Sustain. Energy Rev. **33**, 371 (2014).

42. S. Leblanc, S. K. Yee, M. L. Scullin, C. Dames, and K. E. Goodson, Renew. Sustain. Energy Rev. **32**, 313 (2014).

43. G. Zhang, in *Therm. Thermoelectr. Prop. Nanomater.* (Royal Society of Chemistry, 2014), pp. 101–120.

44. M. Toprak, Y. Zhang, and M. Muhammed, Mater. Lett. **57**, 3976 (2003).

45. M. S. Dresselhaus, G. Chen, M. Y. Tang, R. G. Yang, H. Lee, D. Z. Wang, Z. F. Ren, J. P. Fleurial, and P. Gogna, Adv. Mater. **19**, 1043 (2007).

46. D. Y. Chung, T. P. Hogan, M. R. Lane, P. Brazis, J. R. Ireland, C. R. Kannewurf, M. Bastea, C. Uher, and M. G. Kanatzidis, J. Am. Chem. Soc. **126**, 6414 (2004).

47. C. D. Malliakas, D. Y. Chung, H. Claus, and M. G. Kanatzidis, J. Am. Chem. Soc. **135**, 14540 (2013).

48. D. Y. Chung, S. D. Mahanti, W. Chen, C. Uher, and M. G. Kanatzidis, in *Mater. Res. Soc. Symp. - Proc.* (2003), pp. 141–148.

49. D. Y. Chung, T. P. Hogan, N. Ghelani, P. W. Brazis, M. A. Lane, C. R. Kannewurf, and M. G. Kanatzidis, in *Proc. - IEEE Int. Symp. Circuits Syst.* (2001), pp. 351–356.

50. A. Datta and G. S. Nolas, Eur. J. Inorg. Chem. **2012**, 55 (2012).

51. G. Kieslich, C. S. Birkel, I. Veremchuk, Y. Grin, and W. Tremel, Dalton Trans. **43**, 558 (2014).

52. A. Mani, J. Janaki, A. T. Satya, T. G. Kumary, and A. Bharathi, J. Phys. Condens. Matter **24**, 075601 (2012).

53. P. Sun, M. Baenitz, A. Gippius, A. Herzog, and B. B. Iversen, *Correlation Effects in the Semimetal $FeSb_2$: From Bulk Properties to Spectroscopy (Selected Research Report)* (2009), pp. 37–40.

54. Y. Ma, Q. Hao, B. Poudel, Y. Lan, B. Yu, D. Wang, G. Chen, and Z. Ren, Nano Lett. **8**, 2580 (2008).

55. X. Yan, B. Poudel, Y. Ma, W. S. Liu, G. Joshi, H. Wang, Y. Lan, D. Wang, G. Chen, and Z. F. Ren, Nano Lett. **10**, 3373 (2010).

56. C. B. Vining, Nat. Mater. **7**, 765 (2008).

57. J. H. Roudebush, M. Orellana, S. Bux, T. Yi, and S. M. Kauzlarich, J. Solid State Chem. **192**, 102 (2012).

58. C. W. Myles, K. Biswas, and E. Nenghabi, Phys. B Condens. Matter **401**, 695 (2007).

59. D. Arcon, A. Zorko, P. Jeglic, J. Xu, J. Tang, Y. Tanabe, S. Heguri, and K. Tanigaki, J. Phys. Soc. Japan **82**, 014703 (2013).

60. C. Stiewe, L. Bertini, M. Toprak, M. Christensen, D. Platzek, S. Williams, C. Gatti, E. Müller, B. B. Iversen, M. Muhammed, and M. Rowe, J. Appl. Phys. **97**, 044317 (2005).

61. Z. He, C. Stiewe, D. Platzek, G. Karpinski, E. Müller, S. Li, M. S. Toprak, and M. Muhammed, J. Appl. Phys. **101**, 043707 (2007).

62. M. S. Toprak, C. Stiewe, D. Platzek, S. Williams, L. Bertini, E. Müller, C. Gatti, Y. Zhang, M. Rowe, and M. Muhammed, Adv. Funct. Mater. **14**, 1189 (2004).

63. L. Bertini, C. Stiewe, M. Toprak, S. Williams, D. Platzek, A. Mrotzek, Y. Zhang, C. Gatti, E. Müller, M. Muhammed, and M. Rowe, J. Appl. Phys. **93**, 438 (2003).

64. S. Li, Z. He, M. S. Toprak, C. Stiewe, E. Müller, and M. Muhammed, Phys. Status Solidi - Rapid Res. Lett. **1**, 259 (2007).

65. S. Ahmad, S. D. Mahanti, and M. G. Kanatzidis, in *Mater. Res. Soc. Symp. Proc.* (2006), pp. 161–166.

66. K. Ahn, C. Li, C. Uher, and M. G. Kanatzidis, Chem. Mater. **21**, 1361 (2009).

67. J. Androulakis, Y. Lee, I. Todorov, D. Y. Chung, and M. G. Kanatzidis, Phys. Rev. B - Condens. Matter Mater. Phys. **83**, 195209 (2011).

68. J. Androulakis, I. Todorov, D.-Y. Chung, S. Ballikaya, G. Wang, C. Uher, and M. Kanatzidis, in *Mater. Res. Soc. Symp. Proc.* (2010), pp. 75–80.

69. C. I. Wu, I. Todorov, M. G. Kanatzidis, E. Timm, E. D. Case, H. Schock, and T. P. Hogan, J. Electron. Mater. **41**, 1579 (2012).

70. M. I. Fedorov, J. Thermoelectr. **2**, 51 (2009).

71. S. Battiston, S. Fiameni, M. Saleemi, S. Boldrini, A. Famengo, F. Agresti, M. Stingaciu, M. S. Toprak, M. Fabrizio, and S. Barison, J. Electron. Mater. **42**, 1956 (2013).

72. M. Saleemi, M. S. Toprak, S. Fiameni, S. Boldrini, S. Battiston, A. Famengo, M. Stingaciu, M. Johnsson, and M. Muhammed, J. Mater. Sci. **48**, 1940 (2013).

73. A. Famengo, S. Battiston, M. Saleemi, S. Boldrini, S. Fiameni, F. Agresti, M. S. Toprak, S. Barison, and M. Fabrizio, J. Electron. Mater. **42**, 2020 (2013).

74. P. Jood, R. J. Mehta, Y. Zhang, G. Peleckis, X. Wang, R. W. Siegel, T. Borca-Tasciuc, S. X. Dou, and G. Ramanath, Nano Lett. **11**, 4337 (2011).

75. K. H. Jung, S. M. Choi, C. H. Lim, W. S. Seo, and H. H. Park, Surf. Interface Anal. **44**, 1507 (2012).

76. J. He, Y. Liu, and R. Funahashi, J. Mater. Res. **26**, 1762 (2011).

77. H. Yamaguchi, Y. Chonan, M. Oda, T. Komiyama, T. Aoyama, and S. Sugiyama, J. Electron. Mater. **40**, 723 (2011).

78. A. P. Gonçalves and C. Godart, Eur. Phys. J. B **87**, (2014).

79. O. Appel, M. Schwall, D. Mogilyansky, M. Köhne, B. Balke, and Y. Gelbstein, J. Electron. Mater. **42**, 1340 (2013).

80. C. S. Birkel, J. E. Douglas, B. R. Lettiere, G. Seward, N. Verma, Y. Zhang, T. M. Pollock, R. Seshadri, and G. D. Stucky, Phys. Chem. Chem. Phys. **15**, 6990 (2013).

81. B. Balke, J. Barth, M. Schwall, G. H. Fecher, and C. Felser, J. Electron. Mater. **40**, 702 (2011).

82. L. D. Hicks and M. S. Dresselhaus, Phys. Rev. B. Condens. Matter **47**, 8 (1993).

83. M. S. Dresselhaus, in *Int. Conf. Thermoelectr. ICT, Proc.* (1998), pp. 29–32.

84. M. S. Dresselhaus, G. Chen, Z. Ren, J. P. Fleurial, P. Gogna, M. Y. Tang, D. Vashaee, H. Lee, X. Wang, G. Joshi, G. Zhu, D. Wang, R. Blair, S. Bux, and R. Kaner, in *Mater. Res. Soc. Symp. Proc.* (2008), pp. 29–41.

85. J. P. Heremans, M. S. Dresselhaus, L. E. Bell, and D. T. Morelli, Nat. Nanotechnol. **8**, 471 (2013).

86. M. Zebarjadi, G. Joshi, G. Zhu, B. Yu, A. Minnich, Y. b. Lan, X. Wang, M. S. Dresselhaus, Z. Ren, and G. Chen, Nano Lett. **11**, 2225 (2011).

87. M. Zebarjadi, K. Esfarjani, M. S. Dresselhaus, Z. F. Ren, and G. Chen, Energy Environ. Sci. **5**, 5147 (2012).

88. M. S. Dresselhaus, in *AIP Conf. Proc.* (2013), pp. 36–39.

89. A. J. Minnich, M. S. Dresselhaus, Z. F. Ren, and G. Chen, Energy Environ. Sci. **2**, 466 (2009).

90. S. M. Kauzlarich, S. R. Brown, and G. J. Snyder, Dalt. Trans. 2099 (2007).

91. F. Gascoin, S. Ottensmann, D. Stark, S. M. Haile, and G. J. Snyder, Adv. Funct. Mater. **15**, 1860 (2005).

92. G. S. Nolas, J. Poon, and M. G. Kanatzidis, Mater. Res. Soc. Bull. **31**, 199 (2006).

93. M. Muhammed and M. S. Toprak, in *Thermoelectr. Handb. Macro to Nano*, edited by D. M. Rowe (CRC Press, Boca Raton, FL, 2006), pp. 41–1 to 41–9.

94. J. R. Szczech, J. M. Higgins, and S. Jin, J. Mater. Chem. **21**, 4037 (2011).

95. B. Yu, M. Zebarjadi, H. Wang, K. Lukas, D. Wang, C. Opeil, M. S. Dresselhaus, G. Chen, and Z. Ren, Nano Lett. **12**, 2077 (2012).

96. C. S. Birkel, T. Claudio, M. Panthöfer, A. Birkel, D. Koll, G. Kieslich, J. Schmidt, R. Hermann, and W. Tremel, Phys. Status Solidi **208**, 1913 (2011).

97. G. Geng and K. Kovnir, *Filled Skutterudite Nanocomposites (Research Report),* (2010), pp. 1–28.

98. C. J. Vineis, A. Shakouri, A. Majumdar, and M. G. Kanatzidis, Adv. Mater. **22**, 3970 (2010).

99. C. Zhou, J. Sakamoto, D. Morelli, X. Zhou, G. Wang, and C. Uher, J. Appl. Phys. **109**, 271 (2011).

100. M. Pokharel, M. Koirala, H. Zhao, K. Lukas, and Z. Ren, **1490**, 115 (2012).

101. N. Satyala, A. Tahmasbi Rad, Z. Zamanipour, P. Norouzzadeh, J. S. Krasinski, L. Tayebi, and D. Vashaee, J. Appl. Phys. **115**, 044304 (2014).

102. Y. Ma, R. Heijl, and A. E. C. Palmqvist, J. Mater. Sci. **48**, 2767 (2012).

103. C. Stiewe, Z. He, D. Platzek, G. Karpinski, E. Müller, S. Li, M. Toprak, and M. Muhammed, Materwiss. Werksttech. **38**, 773 (2007).

104. M. S. Toprak, S. Li, and M. Muhammed, in *Modul. Syst. Appl. Thermoelectr.*, edited by D. M. Rowe, 2nd ed. (CRC Press, Boca Raton, FL, 2012), pp. 17–1 to 17–20.

105. J. Schilz, M. Riffel, K. Pixius, and H. J. Meyer, Powder Technol. **105**, 149 (1999).

106. M. Zhou, Z. Chen, and L. Li, Procedia Eng. **27**, 115 (2012).

107. L. D. Zhao, B. P. Zhang, W. S. Liu, and J. F. Li, J. Appl. Phys. **105**, 023704 (2009).

108. M. J. Yang, W. J. Luo, Q. Shen, H. Y. Jiang, and L. M. Zhang, Adv. Mater. Res. **66**, 17 (2009).

109. P. Norouzzadeh, Z. Zamanipour, J. S. Krasinski, and D. Vashaee, J. Appl. Phys. **112**, 124308 (2012).

110. A. J. Zhou, L. D. Feng, W. Liu, X. Y. Dai, H. G. Cui, X. B. Zhao, and J. Z. Li, Mater. Sci. Forum **743-744**, 144 (2013).

111. E. Grob, M. Riffel, and U. Stohrer, J. Mater. Res. **10**, 34 (1995).

112. A. Bentien, S. Johnsen, G. K. H. Madsen, B. B. Iversen, and F. Steglich, Europhys. Lett. **80**, 17008 (2007).

113. M. Koirala, H. Zhao, M. Pokharel, S. Chen, T. Dahal, C. Opeil, G. Chen, and Z. Ren, Appl. Phys. Lett. **102**, 213111 (2013).

114. K. Wei, J. Martin, and G. S. Nolas, Mater. Lett. **122**, 289 (2014).

115. G. Kieslich, C. S. Birkel, I. Veremchuk, Y. Grin, and W. Tremel, Dalton Trans. **43**, 558 (2014).

116. M. E. Anderson, S. S. N. Bharadwaya, and R. E. Schaak, J. Mater. Chem. **20**, 8362 (2010).

117. M. Han, S. Kim, H. Y. Kim, and S. J. Kim, RSC Adv. **3**, 4673 (2013).

118. Y. Zhang, H. Wang, S. Kräemer, Y. Shi, F. Zhang, M. Snedaker, K. Ding, M. Moskovits, G. J. Snyder, and G. D. Stucky, ACS Nano **5**, 3158 (2011).

119. M. Saleemi, M. S. Toprak, S. Li, M. Johnsson, and M. Muhammed, J. Mater. Chem. **22**, 725 (2012).

120. M. Saleemi, M. S. Toprak, S. Li, M. Johnsson, and M. Muhammed, in *AIP Conf. Proc.* (2012), pp. 115–118.

121. M. Saleemi, A. Ruditskiy, M. S. Toprak, M. Stingaciu, M. Johnsson, I. Kretzschmar, A. Jacquot, M. Jägle, and M. Muhammed, J. Electron. Mater. **43**, 1927 (2013).

122. S. Fiameni, A. Famengo, S. Boldrini, S. Battiston, M. Saleemi, M. Stingaciu, M. Jhonsson, S. Barison, and M. Fabrizio, J. Electron. Mater. **42**, 2062 (2013).

123. S. Fiameni, A. Famengo, F. Agresti, S. Boldrini, S. Battiston, M. Saleemi, M. Johnsson, M. S. Toprak, and M. Fabrizio, J. Electron. Mater. **43**, 2301 (2014).

124. M. Saleemi, M. Y. Tafti, M. S. Toprak, M. Stingaciu, M. Johnsson, M. Jägle, A. Jacquot, and M. Muhammed, in *Mater. Res. Soc. Symp. Proc.* (2013), pp. 121–126.

125. M. Saleemi, M. S. Toprak, S. Li, M. Johnsson, and M. Muhammed, in *AIP Conf. Proc.* (2012), pp. 115–118.

126. T. Dasgupta, C. Stiewe, R. Hassdorf, A. J. Zhou, L. Boettcher, and E. Mueller, Phys. Rev. B **83**, 235207 (2011).

127. A. Jacquot and K. Bartholom, *IPM-ZT-Meter-870K : Realtime Measurement of the Figure-of-Merit(http://www.ipm.fraunhofer.de/en)* (2012), pp. 2–3.

128. S. Boldrini, A. Famengo, F. Montagner, S. Battiston, S. Fiameni, M. Fabrizio, and S. Barison, J. Electron. Mater. **42**, 1319 (2013).

129. A. Pfaadt, U. Pelz, K. Kaspar, S. Schmidt, M. Dold, and M. Ja, J. Electron. Mater. **41**, 1851 (2012).

130. M. D. Abràmoff, I. Hospitals, P. J. Magalhães, and M. Abràmoff, Biophotonics Int. **11**, 36 (2004).

131. C. Schneider, W. S. Rasband, and K. W. Eliceiri, Nat. Methods **9**, 671 (2012).

132. M. Scheele, N. Oeschler, K. Meier, A. Kornowski, C. Klinke, and H. Weller, Adv. Funct. Mater. **19**, 3476 (2009).

133. F. Yu, J. Zhang, D. Yu, J. He, Z. Liu, B. Xu, and Y. Tian, J. Appl. Phys. **105**, 094303 (2009).

134. M. Akasaka, T. Iida, T. Nemoto, J. Soga, J. Sato, K. Makino, M. Fukano, and Y. Takanashi, J. Cryst. Growth **304**, 196 (2007).

135. J. Y. Jung and I. H. Kim, Electron. Mater. Lett. **6**, 187 (2010).

136. J. J. Martin, J. Phys. Chem. Solids **33**, 1139 (1972).

137. M. Saleemi, M. S. Toprak, S. Fiameni, S. Boldrini, S. Battiston, A. Famengo, M. Stingaciu, M. Johnsson, and M. Muhammed, J. Mater. Sci. **48**, 1940 (2012).

138. S. W. You, K. H. Park, I. H. Kim, S. M. Choi, W. S. Seo, and S. U. Kim, J. Electron. Mater. **41**, 1675 (2011).

139. S. K. Bux, M. T. Yeung, E. S. Toberer, G. J. Snyder, R. B. Kaner, and J. P. Fleurial, J. Mater. Chem. **21**, 12259 (2011).

140. I. Opahle, A. Parma, E. J. McEniry, R. Drautz, and G. K. H. Madsen, New J. Phys. **15**, 105010 (2013).

141. Y. Sadia and Y. Gelbstein, J. Electron. Mater. **41**, 1504 (2012).

142. A. Famengo, S. Battiston, M. Saleemi, S. Boldrini, S. Fiameni, F. Agresti, M. S. Toprak, S. Barison, and M. Fabrizio, J. Electron. Mater. **42**, 2020 (2013).

143. T. Itoh and M. Yamada, J. Electron. Mater. **38**, 925 (2009).